Author:
Wang, Chenhao

Title:
Morphologically engineered silver phosphate with polymer and ionic liquids to enhance photoactivity

Morphologically engineered silver phosphate with polymer and ionic liquids to enhance photoactivity

Chenhao Wang
MSc by research Chemistry

October 2019

This thesis is submitted in partial fulfillment of the requirements for the degree of MSc by research Honors Chemistry at the University of Bristol.

Abstract

Two different strategies are investigated to control the size and morphology of silver phosphate (Ag_3PO_4) crystals to improve the photoactivity in water photooxidation. In aqueous crystallization reactions the biopolymer additive carboxymethyl dextran sodium (CM Dextran sodium) could decrease the particle size and regulate the morphology of Ag_3PO_4. The Ag_3PO_4 with smaller and uniform shape evolved more oxygen under visible light irradiation when using $AgNO_3$ as sacrificial agent. Non-aqueous synthesis of Ag_3PO_4 with mixtures of the ionic liquids (1-butyl-3-methylimidazolium acetate [BMIM](OAc) and 1-butyl-3-methylimidazolium dihydrogen phosphate [BMIM]H_2PO_4)) is reported for the first time. The effect of reactant concentration and temperature on crystal morphology were systematically investigated. An optimum set of conditions was found for producing crystals with a unique morphology. The higher surface area of these crystals was reflected in enhanced oxygen evolution and photostability compared to all other ionic liquid and biopolymer systems tested. The project studied the interaction between ionic liquids with inorganic reactants and the influence of water addition to the Ag_3PO_4 formation. In conclusion, through controlling the size and morphology, polymer (CM Dextran sodium) and ionic liquids could remarkably enhance the photoactivity of Ag_3PO_4.

Acknowledgements

Sincerely thanks Dr Sean Davis and Dr Avinash Patil for the guidance in my master research thesis and for providing me with the help and training in laboratory works.

Thanks to Prof Charl FJ Faul and his group for the help of Brunauer-Emmett-Teller (BET) test.

Declaration

All the synthesis and characterizations are operated independently. Brunauer-Emmett-Teller (BET) is tested with the help of Faul group.

Content

Introduction

1. The importance of photocatalysis

1.1. The definition and evolution of photocatalysis.

From the industrial age, the requirement of energy consumption has increased significantly, however, reserves of traditional non-renewable energy sources, like coal and fossil oil, is facing serious challenge. Therefore, after the energy crisis in 1970s, the research of renewable energy sources, such as sunlight, wind and geothermal heat [1], became attractive. Because of environmental and location limits, wind, tide and geothermal heat energy cannot apply widely, sunlight energy become an ideal choice in general. As intermediate to convert sunlight energy into usable energy, photocatalyst is the core of photocatalysis research. Photocatalysts are materials that absorb sunlight and convert it to chemical energy [2]. From 1911, zinc oxide was found to be able to degrade Prussian blue under illumination, which is the first time scientist notice photocatalysis [3]. Then Fujishima and Honda [4] firstly reported water photooxidation phenomenon happened on the surface of TiO_2 under ultra-violet light, and various semiconductors including metal oxides [5], non-metal oxide [6], sulphides [7], nitrides [8] and phosphates [9], were synthesized to optimize activity, stability and efficiency of photocatalyst in past decades. In further research, synthesis of an efficient photocatalyst with appropriate band gap, high stability and long-term activity is the target of photocatalysis study.

Beside renewable energy, photocatalysis is also widely applied in many other fields. For example, in the pollution abatement, photocatalyst has impressive performance on wastewater purification and organic dye degradation [10]. Rather than traditional pollutant absorption and sediment by porous materials, like activated carbon, chemical reaction happens in pollutant degradation by photocatalysts, which turns the chemicals to totally harmless. However,

improvement on purification and degradation efficiency and recyclability of photocatalyst are aims for future research.

1.2. The principle of photocatalysis

The essence of photocatalysis is photoreaction acceleration which convert sunlight energy to chemical energy. As shown in figure 1, in a photocatalyst, after absorbing energy from sunlight photon, electrons on valance band transfer to conduction band and left a photo induced hole containing positive charge, then photo induced electrons and holes move to surface of photocatalyst and occur redox reactions with other chemicals [11]. Therefore, photocatalysis could be separated into three steps which are electron excitation, electron and hole migration and redox reactions on surface.

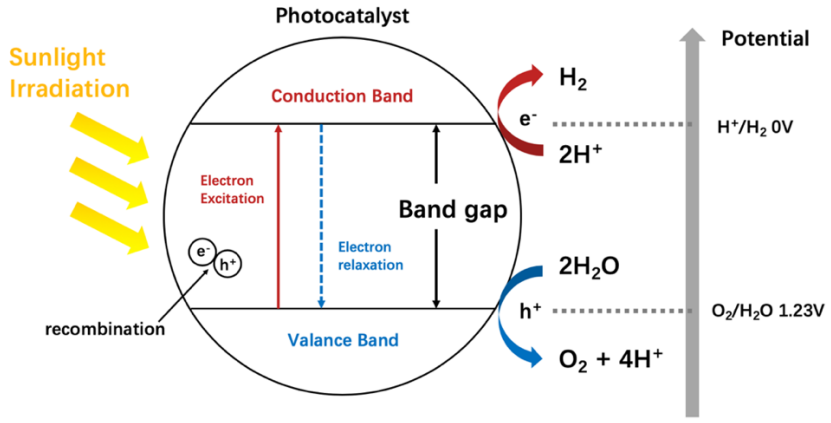

Figure 1. The mechanism of photocatalysis under sunlight irradiation.

There are also plenty of challenges in each step. 1) For electron excitation step, energy absorption essentially depends on the band gap of photocatalyst. Band gap is the minimum energy distance that an excited electron needs to overcome for transferring from valance band to conduction band [12]. The relationship between light wavelength and band gap could be illustrated by Planck equation (shown as equation 1). Based on the equation, due to Planck number and light speed are constant, energy *E* could be calculated through wavelength λ. For example, the wavelength range of ultra-violet light is from 290nm to 400nm, which corresponds to energy range from 4.27eV to 3.10eV

and visible light which wavelength between 400nm and 760nm corresponds to energy range from 3.10eV to 1.63eV [13]. Therefore, the band gap of a light-responding semiconductor must be in the range that the light wavelength corresponds with. Compared with the UV light responding photocatalyst, visible light responding photocatalyst is more desirable. Because, in the sunlight, UV light just occupies about 5%, but visible light takes up over 40% [13], which means the sunlight could be used more efficiently.

$$E = h\nu = \frac{hc}{\lambda}$$

Equation 1. E is the gap energy in joules, h is Planck's constant ($6.62*10^{-34}$ J s), υ is the frequency in hertz, c is the speed of light ($2.998*10^{8}$ m s-1) and λ is the wavelength in meter.

2) In electron and hole migration process, recombination between electrons and holes is the most serious problem, which considerably reduces photocatalysis efficiency. After electrons and holes were formed inside the photocatalyst particle, they need to move to particle surface for following redox reaction. However, without modification, electrons and holes move disorderly, then probability that electrons and holes collide together will be large. Therefore, lowering the recombination probability is important to increase activity of photocatalyst. 3) As the last step of photocatalysis, redox reactions occurring between electrons and holes with other chemicals finally turn sunlight energy to chemical energy. Hence, number of active sites on the surface decides the activity of photocatalysts. Therefore, larger surface area and higher energy exposed crystal facet could develop the performance of photocatalysts [14].

1.3. Development of photocatalysts

According to principle of photocatalysis, photocatalyst development methods can also be concluded into three main directions, which are band gap modification, reduction of recombination and surface active site increase.

1.3.1. Bandgap modification

As prerequire of photocatalysis, band gap is especially vital for photocatalyst. Beside deciding a photocatalyst to be responded by UV light or visible light, band gap also determine which type of redox reaction can occur on the surface of the photocatalyst. For example, as shown in figure 2, TiO_2 anatase, SnO_2 and ZnO are typical UV light responding semiconductors, and CdS, Cu_2O, Fe_2O_3 and Bi_2WO_6 are visible light responding. Then, based on the position of valance band and conduction band, different photocatalysts prefer to happen distinct redox reaction. For instance, the valance band of Bi_2WO_6 locates at around +3.2V vs. NHE (Normal Hydrogen Electrode, pH 7), hence, it is sufficiently associated with oxidation reaction, such as water and carbon dioxide oxidation. However, the conduction band of Bi_2WO_6 locates approximately at +0.5V vs. NHE (pH 7), which means it cannot reduce protons to hydrogen gas [18]. On the contrary, Cu_2O performs well in chemical reduction, but cannot complete water oxidation to produce oxygen [16]. Furthermore, photocatalyst, like g-C_3N_4, can be used for overall water splitting [17]. However, except band gap, the cost and synthesis method of a photocatalyst are also important aspects needed to be considered. Therefore, band gap adjustment is an effective to improve photocatalytic property. The common methods to alter band gap include doping [18] and combination with other catalyst to form heterojunction [19]. Doping is a method that introduces impurity to intrinsic semiconductor to change the electrical property. With mild and moderate doping, the material becomes extrinsic semiconductor which shows some novel electrical property. However, with high level doping, the material turns to degenerate semiconductor that present more like metallic materials.

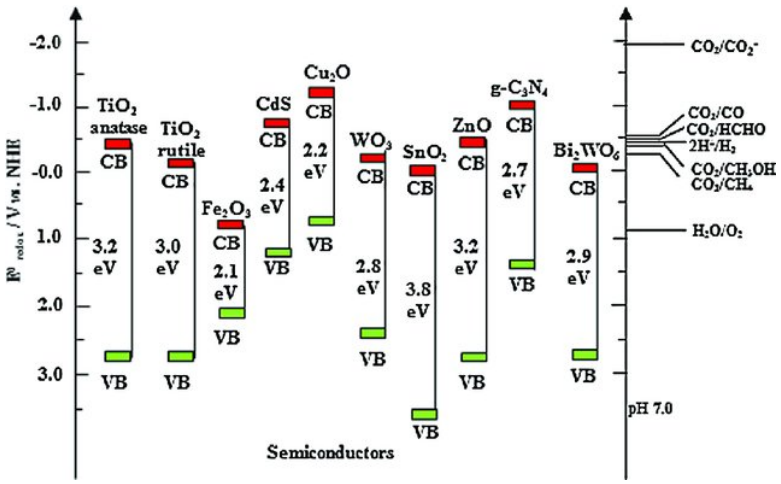

Figure 2. Band gap of photocatalysts with respect to the redox potential of different chemical species measured at pH at 7. Adapted from Refs. [15-18].

1.3.2. Use of cocatalysts

After electrons and holes are induced, transferring to surface more rapidly and avoiding the recombination could significantly improve photocatalytic activity. Modifying the surface of semiconductors with metal nanoparticles is a quite useful way to accelerate the electron transfer as cocatalysts. The metal being used are always noble metal like Pt, Pd, Au and Ni that possess lower Fermi level. Therefore, Schottky junction is formed, then electrons tend to aggregate to the metal and occur the further reactions.

Another method to effectively avoid the recombination is mixing two semiconductors with different energy band structure for producing the heterojunction to form the dual semiconductor photocatalyst system. Furthermore, the heterojunctions could be separated into three types. As shown in figure 3, in type A, the conduction band (CB) of semiconductor 1 (S1) is higher than the CB of semiconductor 2 (S2), but the valance band (VB) of S1 is lower than the VB of S2. Therefore, both the electrons and holes tend to move forward to S2; in type B, the CB of S1 is still higher than S2, however, the VB of S1 is higher than S2, then the electrons transfer to S2 and holes transfer to S1, hence electrons and holes aggregate into different semiconductors and the possibility of recombination could be reduced. For

type C, both CB and VB of S2 is higher than S1, but because the difference between the energy bands is large, the exchange migration of electrons and holes need to pass through an electron mediator, but electrons and holes will recombine in the process. In summary, forming a semiconductors combination of type B is the target to improve separation of electrons and holes [20].

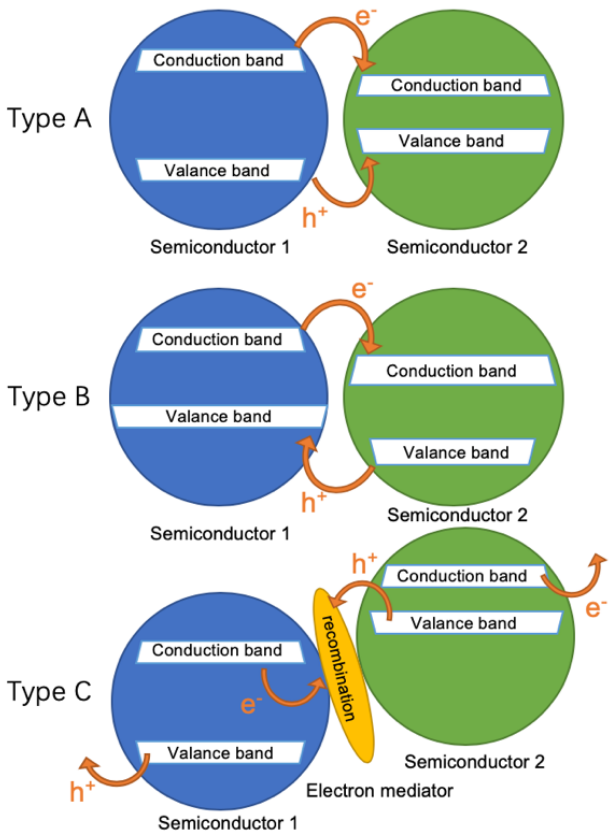

Figure 3. Three different types of semiconductors combination to form heterojunctions.

3) When electrons and holes getting to the surface of photocatalysts, a larger surface area and more active sites are factors for developing the activity. There are plenty of methods to extend the surface area of photocatalysts. Synthesizing photocatalyst nanoparticles and photocatalyst with special morphology could both increase surface area. For example, Wei [21] produced a TiO_2 with extremely large surface area via a hydrothermal method using cetyltrimethylammonium bromide as the template. The TiO_2 with large surface area presented considerably enhanced photoactivity. Beside this,

forcing photocatalyst crystals to exposure high energy facet could also benefit the redox reactions occurred on the surface. For instance, David [22] reported a facet engineered Ag_3PO_4 that showed extraordinary performance in water photooxidation. The facet exposure of Ag_3PO_4 was guided by theoretical modelling.

1.4. The advantages and limits of silver phosphate

Silver phosphate was firstly reported as photocatalyst by Yi [23] in 2010. Under visible light irradiation, Ag_3PO_4 could form photo-induced electrons and holes easily and possess excellent photocatalytic oxidation ability, and it can produce O_2 through water splitting and effectively degrade organic dye, like Methylene Blue and Rhodamine B. Then, compared with $BiVO_4$ and N-TiO_2, Ag_3PO_4 presents better performance with same experimental conditions. The valance band of Ag_3PO_4 locates at 2.85eV, which is higher than the oxidation potential of H_2O/O_2 (1.23eV). Therefore, holes h^+ could directly oxidize the absorbed H_2O molecules to release oxygen gas. The conduction band of Ag_3PO_4 locates at 0.45eV, which is higher than the reduction potential of H^+/H_2. Thus, without sacrificial agent, photo-induced electrons react with silver cations to form Ag^0 particles. And the band gap of Ag_3PO_4 is 2.43eV, which means it could absorb the sunlight with wavelength shorter than 530 nm. In the range from 400 to 480nm of visible light, the quantum yield is over than 90%. The great photoactivity of Ag_3PO_4 is because of its special energy band structure. Firstly, Ag_3PO_4 could be regarded as Ag_2O lattice doped with non-metallic element P, the bottom of conduction band is hybridized by Ag 5s, 5p and few P 3s orbitals, and the top of valance band is hybridized by Ag 4d and O 2p orbitals, hence the doping of P element broadens the band gap of Ag_2O. Then the formation of PO_4^{3-} tetrahedrons weakens Ag-O covalent bond and restrain the hybridization between Ag d and O p orbitals, which formed highly dispersed Ag s-Ag s hybridization and delocalized electrons and promote electron transfer to the surface of Ag_3PO_4.

Highly dispersed conduction band and inductive effect of PO_4^{3-} could make electrons/hole separation more effectively. However, because the electrons are easily to reduce Ag^+ ions to Ag^0 particles and lower the activity of photocatalyst, the photocatalytic reaction always happens in the solution with sacrificial agent containing Ag^+ ions. Furthermore, compared with other photocatalysts, the cost of Ag_3PO_4 is higher, which limits the application in the industrial. Therefore, the modifications to the Ag_3PO_4 focus on 3 aspects, which are photoactivity improvement, stability development and cost reduction. Accordingly, there are some main strategies for improve Ag_3PO_4. 1) control of morphology, particle size and crystal structure, which could shorten the distance for electrons and holes transferring to surface, exposure more high energy crystal facet and extend surface area. 2) metal sediment on the surface, which develop the light adsorption and electron transfer. 3) combination with other semiconductors to adjust energy band structure, which expand light absorption range and oxidation/reduction potential. 4) loading the Ag_3PO_4 to a suitable carrier could improve adsorption ability and recyclability of the novel Ag_3PO_4 carrier system.

1) Morphology control: photocatalysis reactions happen on the surface of photocatalyst, thus the photocatalyst morphology, like particle size, crystal facet, specific surface area and pore structure, influence photoactivity and stability significantly. Due to large surface area and higher number of defect sites, nanosized catalysts typically possess greater activity. The order of crystal facet energy of Ag_3PO_4 is {111} > {110} > {100}, and crystal face energy correlates with active sites on the surface of catalyst. Therefore, controlling facet exposure by adding surfactants, templates or changing experimental conditions is a main direction to control the morphology of Ag_3PO_4. There are already several shapes of Ag_3PO_4 have been formed (shown as Figure 4). For examples, Bi [24] used different Ag^+ precursor react with Na_2HPO_4 to form Ag_3PO_4

with distinct morphologies. Using CH_3COOAg as precursor, Ag_3PO_4 rhombic dodecahedron exposing {110} facet was produced, then, the cubic Ag_3PO_4 exposing {100} facet was formed with $[Ag(NH_3)_2]^+$ as precursor. And because Ag_3PO_4 rhombic dodecahedron exposed facet with higher surface energy, it showed wider visible light responding range and better photoactivity. Furthermore, the different phosphate ligands also influenced the final Ag_3PO_4 morphology. Bi [25] also used H_2O_2 to oxidize Ag nanowire with addition of polyvinyl pyrrolidone (PVP) to yield 2-dimensional dendritic Ag_3PO_4. This is because PVP could selectively absorb on the surface of Ag_3PO_4 and change the direction of crystal growth. With assistance of PVP, Colin [26] used oxidized Ag sheet to react with Na_2HPO_4, to create Ag_3PO_4 tetrahedrons exposing {111} facets. Beside this, Wang [27] produced tetrapod-like Ag_3PO_4 using H_3PO_4 and $AgNO_3$ via hydrothermal method with urea. Urea could form CO_2 and NH_3 at high temperature, then the gases could selectively be absorbed to some certain facet for restraining the crystal growth, which accelerate the growth of {110} facet with higher surface energy.

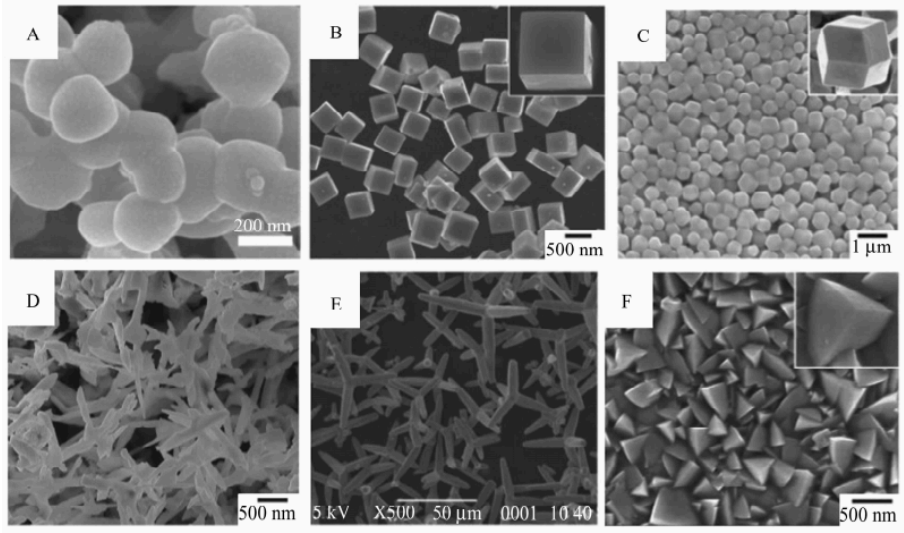

Figure 4. Scanning electron micrographs showing range of morphologies of silver phosphate synthesized with different methods. A) spherical B) cubic C) rhombic dodecahedron D) dendritic E) tetrapod F) tetrahedral. [25-27]

2) Noble metal sediment: Through induction by UV or visible light, nanosized noble metallic particles could rise resonance scattering. Therefore, using localized surface plasmon resonance effect, noble metal sediment on semiconductor surface could effectively broaden the light adsorption range. Simultaneously, noble metal could easily capture electrons until the Fermi energy level of metal nanoparticles and semiconductors become equal, which could reduce the recombination between electrons and holes and make the holes produce more active oxides to degrade pollutant. Then, photocorrosion of Ag_3PO_4 can cause Ag metallic particles formation on the surface, hence the Ag/Ag_3PO_4 composite is the most popular system in photoactivity research. For example, Wang [28] studied the influence of metallic silver sediment on the photoactivity, based on the circulation rounds of Ag_3PO_4 photooxidation reaction. Within 4 times circulation, the few metallic Ag^0 formed core-shell structure with Ag_3PO_4, and electron traps were produced, which could accelerate the transfer of photo-induced electrons. Furthermore, following with the increase of circulation rounds, the surface area of Ag_3PO_4 also enlarged, which improve the absorption of organic dye. However, with more than 4 times repeat catalysis reactions, excess silver particles avoid the light absorption of Ag_3PO_4. Therefore, the photoactivity was reduced with more circulations.
3) Combination with other semiconductors: Based on the energy band theory, the combination between Ag_3PO_4 and other semiconductors could form heterojunctions. Refactoring energy band structure can restrain the recombination and improve photoactivity. Figure 5 shows 4 main types of Ag_3PO_4-semiconductor composites. 1) Type A is combination between Ag_3PO_4 with UV light-responding semiconductor with higher valance and conduction band. For example, Xie [29] combined Ag_3PO_4 with TiO_2 by loading Ag_3PO_4 nanoparticles onto surface of TiO_2. Then photo-induced electrons of Ag_3PO_4 was excited and

transferred from valance band to conduction band, but the holes transferred from the valance band of Ag_3PO_4 to the valance band of TiO_2 that possesses lower electrical potential, which avoided the recombination. Furthermore, the combination with TiO_2 could reduce the dosage of silver, thus the cost of entire catalyst composite will be lower. 2) Type B is combination between Ag_3PO_4 with UV light-responding semiconductor with lower valance and conduction band. In contrast to type A, after electrons and holes were induced, electrons transition from the conduction band of Ag_3PO_4 to the conduction band of semiconductor with the lower electrical potential conduction band, like SnO_2, could achieve the effective separation of electrons and holes. 3) Type C is combination between Ag_3PO_4 with visible light-responding semiconductor with higher valance and conduction band. Cao [30] synthesized the AgBr/Ag_3PO_4 heterogeneous catalyst. Because AgBr and Ag_3PO_4 have similar band gap, they can be simultaneously excited, then electrons tend to move forward Ag_3PO_4 and holes tend to transfer to AgBr. Thus, the recombination could also be prevented. 4) Type D is the combination between Ag_3PO_4 with visible light-responding semiconductor with lower valance and conduction band, which is similar as type C but with opposite electron/hole transition direction. This type composite includes combination between Ag_3PO_4 with Bi_2WO_6, WO_3 and $BIVO_4$ [31].

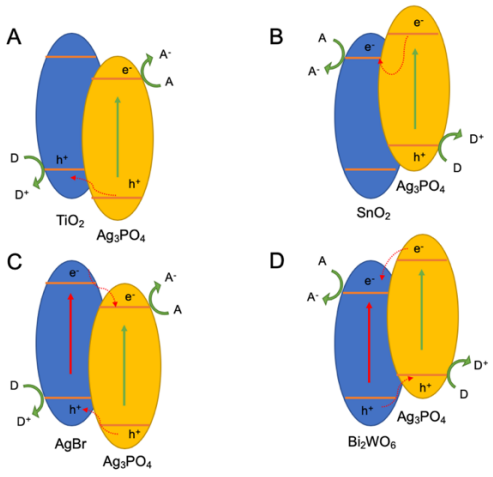

Figure 5. four different types of Ag_3PO_4/semiconductor composites.

4) Composite with other carriers: Combining Ag_3PO_4 with carriers possessing high absorption ability and electrical conductivity or containing active ligands is also an ideal method to improve photoactivity. Xiao [31] used the active sites uniformly distributing inside the chitosan(CS) molecules as soft template to produce Ag_3PO_4. Ag^+ forms chelation with the soft template firstly, then the special 3-dimensional structure and molecular conformation of different molecular weight chitosan control the synthesis of Ag_3PO_4 nanoparticles. With CS0, CS4, CS6 and CS8, Ag_3PO_4/CS nanocomposites with different morphology were formed. The morphology structure and photoactivity all depend on the molecular weight of CS. Following with the decrease of molecular weight, the surface area and pore size of the composite increased. The morphology of composite also turns from core-shell structure to flower-like hollow structure, and the composite showed considerable performance in photoactivity and stability.

Inorganic systems for many applications require particle size and morphology control to improve properties and achieve some special functions. Materials for photocatalysis is one example where this is particularly important. In this thesis, Ag_3PO_4 was used for water photooxidation which is a key component of water splitting. Water splitting is one of the most important and meaningful applications of photocatalysis. And the water splitting could be divided into two parts which are H_2 production and O_2 production. Because every H_2 molecule production requires 2 electrons, but every O_2 molecule production requires 4 holes, which means, compared with H_2 photoreduction, the water photooxidation is harder to be achieved. Therefore, synthesizing an effective photocatalyst for water oxidation is both vital for oxygen production and the further entire water splitting reaction. Due to appropriate band gap, silver phosphate is a great catalyst for the research of photooxidation under visible light. In the experimental, CM Dextran sodium and ionic liquids were applied

to control the morphology of Ag_3PO_4 and improve the photoactivity of water oxidation.

2. Polymers in inorganic material synthesis

There are large number of inorganic semiconductors used as photocatalysts, and the morphology of the materials plays an important role in the photoactivity improvement. To control the crystal structure and morphology of photocatalyst, many types of materials are applied to the synthesis system, such as inorganic salt [32], inorganic acid (base) [33], organic acid [34], alcohol [35], amino acid [36], protein [37], sugar [38] and other polymers with special structure. For polymer materials, through molecular design and optimization, they can react as surfactant or soft template. Polymers could not only present hydrophilic or hydrophobic property on the interface between oil and water, but also selective absorption of minerals and metals in aqueous solution. Numerous polymers could be used as surfactant or template, however as morphology and crystal structure controlling agent, most researches focus on biopolymers, double hydrophilic block copolymers, dendritic polymers and polymer electrolyte.

In the synthesis of inorganic materials, biopolymers can control the nucleation and crystal growth. For the formation of biopolymer-inorganic hybrid material, the reaction could happen both in situ and ex situ. With different combination methods between biopolymers and reactants, the morphology and crystal structure of the final product will be significantly distinct. When the biopolymer and inorganic material react in situ, biopolymers could present several different functions, such as controlling agent, support, scaffold and nanocontainer [39]. As controlling agent, biopolymer could guide the growth of specific crystal facet. For example, Franco [40] used oligopeptide as controlling agent in calcium oxalate (CaC_2O_4) synthesis to elongate the (100) facet, and the chain length of oligopeptide could directly influence the morphology of CaC_2O_4. Therefore, biopolymers are widely used in the bio mineralization for altering the morphology

and facet exposure. Then the special structure and various functional groups allow biopolymers act as supports in the inorganic synthesis. For instance, Pu [41] produced hollow porous cadmium sulfide (CdS) with DNA on the silica beads. After treating surface -OH groups on silica beads with 3-Aminopropyl-trimethoxysilane (APTMS), the amine-functionalized beads absorbed DNA. Then the Na_2S and $Cd(ClO_4)_2$ were added and CdS nanowires grew on the surface of the beads. Finally, the beads were removed by NH_2F and HF and the hollow porous CdS was formed. Furthermore, biopolymers can also work as the soft template and scaffold to yield products with some simple morphologies, like spherical droplet, because the biopolymers could aggregate together and form certain shape through chelation effect and electrostatic interaction. Compared with reacting as support, when the production of materials occurred in the network of polymers rather than the edge, the biopolymer is regarded as scaffold.

As outlined in Section 1.4 the biopolymer chitosan has previously been used as a soft template to control Ag_3PO_4 crystal growth. Surprisingly there are no literature reports of comparable studies with dextran polymers. Carboxymethyl-dextran sodium (CM Dextran sodium) has been widely used in crystal engineering studies. As shown in figure 6, the main chain structure of CM Dextran sodium is similar with Dextran. With the additional carboxylic acid functional groups, the polymer could work as soft template in the synthesis of Ag_3PO_4. The abundant hydroxyl and carboxylic groups could chelate with silver ions and influence the further crystal nucleation and growth.

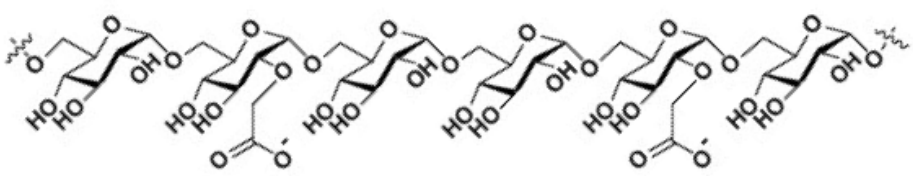

Figure 6. The structure of carboxymethyl-dextran sodium (CM Dextran sodium).

3. Ionic liquids in organic synthesis

Most traditional chemical reactions occur in the solvents, and various organic solvents are most common reaction medium. Organic solvent could dissolve compounds effectively and allow the reactions happen, however it is not environmental-friendly, due to the toxicity and volatility. Therefore, finding a green solvent for the chemical industrial is necessary and urgent. As a typical green solvent, ionic liquids are attempted to be applied in many fields. Ionic liquid is the liquid only consisting of cations and anions at room temperature. It is always composed by organic cation containing N and P elements and inorganic anions, such as imidazolium, pyridinium, alkylammonium and alkyl phosphonic acidic salt (The structures of the common cations in ionic liquids are shown as Figure 7) [42].

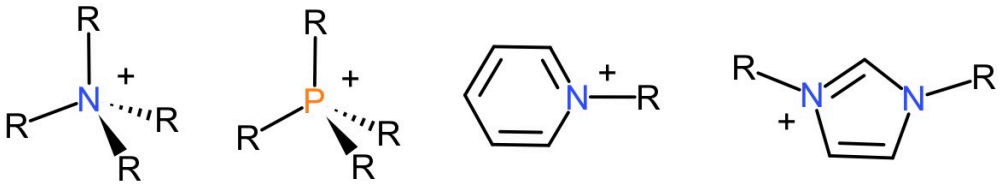

Figure 7. The structure of 4 common cations in ionic liquids; alkylammonium, alkyl phosphonic acidic, pyridinium, imidazolium cations.

There are many significant advantages of ionic liquids that cannot be replaced by other solvents. 1) Ionic liquid possesses very low vapor pressure and it is non-volatile, flammable and toxic. Therefore, it could be used in vacuum system and not harmful to environment. 2) Ionic liquid can dissolve plentiful polar or non-polar organic and inorganic materials, then it is readily to be separated with other materials and could be recycled. Beside this, because of the immiscibility of ionic liquid with some organic solvent, it can provide a non-water polarity adjustable two-phase system. 3) The thermostability and chemical stability of ionic liquid are both considerable, which allow it keep in liquid phase in a wide temperature range (from -96^{o}C to about 400^{o}C) [43]. Therefore, ionic liquids are beneficial to the thermodynamic control. 4) Most ionic liquids possess high conductivity and a large

potential window which could reach to 4V. Due to all the features outlined above, ionic liquids are widely used in separation [44], catalysis [45] and electrical chemistry [46]. However, compared with organic research, the reports about inorganic synthesis with ionic liquids are not abundant. For producing desired inorganic materials with special morphology or feature always require some toxic solvent or templates and under some serious reaction conditions. Therefore, a more effective, environmental-friendly and easier synthesis method is required, Fortunately, ionic liquid meets most requirements for the inorganic synthesis. 1) Ionic liquids possess polarity, because of the low surface tension, it could mix well with other phases [47]. Then the low surface tension increases nucleation rate of inorganic materials, which allows the synthesis of particles with smaller size [48]. 2) The low surface energy of ionic liquids could increase stability of the materials dissolving in ionic liquids, and simultaneously improve solubility. Then ionic liquids provide polarity for hydrophobic groups and directing groups, the polarity forces the groups to be parallel or vertical to surface of the dissolving materials. In brief, reacting in ionic liquids can be regarded as reacting in pure ligands [49]. 3) Because of high thermal and chemical stability of ionic liquids, reactions can occur in non-pressure vessels over 100^{o}C. 4) Under non-moisture condition, with assistance of ionic liquids, polar reactants are beneficial to inorganic material synthesis. Because the conditions could avoid formation of hydroxides and amorphous substance. Then external water addition shifts the reaction equilibrium in single direction, which could allow material crystallization [50]. 5) Another important feature of ionic liquids is that they can form extended hydrogen bond in liquid phase and provide a great structure system, thus ionic liquid is also a type of supramolecular solvents [51]. The structure of solvent is also the basis of molecular recognition and self-assembly, beside this, through entropy-driven, materials synthesized in ionic liquids could possess organized structure [52]. There are also some limits of ionic liquids in synthesis. For example, the synthesis of some nitrides and carbides needs high temperature and pressure. The low vapor makes the ionic liquids not suitable for these reactions. However, in recent years, ionic liquids were

still used to yield many special inorganic materials.

1) Porous materials: Aerogel is a type of porous material that possess low density , large specific surface area and low thermo-conductivity, therefore, it is widely used in insulator, optical device and catalyst. In [EMIM][Tf_2N] ionic liquid, Zhen [53] produced stable SiO_2 aerogel with TMOS via sol-gel method. During the aging process of aerogel synthesizing via traditional sol-gel method, the volatilization of solvents could lead the shrink and broken of gel, and the stable sol-gel network cannot be formed. On the contrary, because ionic liquids possess low vapor pressure, long aging time and stronger ionic bond, they could increase yield percentage and stabilize the aerogel network. Furthermore, the solubility of ionic liquids is strong, therefore, they could form the stable and uniform solution with the precursor of the aerogel. Because there is no obvious phase interface between gel and ionic liquids, the products could be formed more effectively. Beside this, there are already many researches about the synthesis of mesoporous material (aperture larger than 2nm) and molecular sieve (aperture usually smaller than 1nm) with surfactant. However, the porous materials with aperture between 1 to 2nm are taken little attention. This type porous material possesses size and morphology selectivity of the organic molecules which particle size is larger than pore size of molecular sieve. Then mesoporous materials are rarely used for the catalysis reaction that requires size selection, because the size of most catalysts is smaller than the pore size of mesoporous materials. Therefore, the porous materials with 1-2nm aperture could meet all the requirements above. Therefore, the porous materials could be applied to catalysis, synthesis of separation membrane and sensor. For example, Wang [54] synthesized highly aligned layered ultra-microporous SiO_2 via nano-casting technique with an amphiprotic ionic liquid [C_{16}mim] Cl as template. The pores in the layered SiO_2 are parallel, and the pore aperture is 1.3nm, the surface area is 1340m^2g^{-1}. After removing ionic liquid template, the SiO_2 skeleton did not collapse. Then, Emily [55] produced $AlPO_4$ zeolite with

ionic liquid and eutectic mixture and four different net structures were yielded with imidazolyl ionic liquids. Because the vapor pressure of room temperature ionic liquid could be ignored, the reactions could happen at normal pressure, which is safer than hydrothermal method. In the $AlPO_4$ zeolite synthesis , ionic liquid not only work as solvent, but also provide cations for inorganic skeleton frame. The interaction between the cations and net frame caused strong template effect, which improve the formation of the zeolite. Furthermore, the structure of the zeolite synthesized in ionic liquids is different with the zeolite produced with hydrothermal method. In the ionic liquids, the zeolite structure could be altered by changing the molecular structure of solvent. Tewyn [56] used $[C_{14}mim]Br$, $[C_{16}mim]Br$ and $[C_{18}mim]Br$ as templates to form porous SiO_2 nanoparticles in spherical, rod-like and tube-like shape, which proved that the microporous structure of SiO_2 could be adjusted through changing alkyl chain length of the ionic liquid.

2) Nanoparticles and hollow spheres: The transition metal nanoparticle dispersing uniformly in the organic solvent or water is becoming an important catalyst in reactions. The catalytic activity and selectivity of the transition metal nanoparticle is different from the traditional heterogeneous and homogenous catalysts. The synthesis of transition metal nanoparticles is usually through the reduction by CO and H_2 with surfactant, polymer and ions as stabilizer. Ionic liquids could synthesize and stabilize transition metal nanoparticles as solvent, because of the ignorable vapor pressure, thermal, chemical and electrical stability. Simultaneously, compared with water-organic two-phase catalysis system, transition metal nanoparticle-ionic liquid system could be separated easily and recycled. For now, Ir [57], Rh [58] and Pd [59] nanoparticles have already been synthesized in ionic liquids. Beside this, nanoparticles could be produced through functionalizing the ligands of ionic liquids. Kim [60] created Au and Pt nanoparticles via imidazolyl ionic liquid containing thiol group. Itoh [61] produced Au nanoparticles (diameter is about 5nm) with imidazolyl ionic

liquid containing thiol group. Through altering the anions of ionic liquids, the hydrophilicity and hydrophobicity of ionic liquids were changed, then the property of nanoparticles produced in ionic liquid also become different. Laura [62] yielded Ag nanoparticles in [BMIM](BF_4), the ionic liquids in the reaction not only worked as modifier, but also prevent the aggregation of nanoparticles.

TiO_2 nanocrystal is used widely in liquid solar cell and photocatalysis. Because the sol-gel reactions always happen in the mixed solvent containing high moisture, which leads the formation of amorphous TiO_2. However, the amorphous TiO_2 does not possess the required electrical property and needs a high temperature for recrystallizing, which may destroy the original structure. Therefore, the synthesis of TiO_2 under room temperature is a field where the ionic liquids could be applied. Zhao [63] synthesized TiO_2 anatase crystals in [BMIM](BF_4) ionic liquids under a mild reaction condition. Another advanced feature of ionic liquids is the low surface tension. The low surface tension could improve the nucleation rate and yield smaller particles. Choi [64] used hydrophobic ionic liquid [BMIM](PF_6) to produce TiO_2 anatase nanoparticles via sol-gel method. The TiO_2 crystal contains large surface area and stable porous structure, which has a great potential in solar energy transfer, photocatalysis and photoelectrical devices. Nakashima [65] introduced [BMIM](PF_6) to $Ti(OBu)^{4-}$ toluene solution system and formed TiO_2 anatase hollow spheres vis interface sol-gel method. Then, by modifying the inner and outer surface of TiO_2 hollow spheres with carboxylic acid and metal nanoparticles, the TiO_2 spheres could present some special functions and be applied in photocatalysis. The method can also be used in the synthesis of other active metal oxides, like the hollow oxide spheres of zirconium, hafnium and niobium.

3) One-dimensional materials: Due to the special physical and chemical property, one-dimensional 1D material are widely used in photoelectrical devices. There are many methods for the synthesis of 1D materials, but they always involved

with toxic surfactant, high reaction temperature and long reaction time. Therefore, a rapid, low temperature, non-template and environmental-friendly synthesis method is desired. Combining the ionic liquid and microwave heat, many 1D materials were produced. Under the microwave radiation, because of the large imidazolyl and pyridine ligand cation ions, the high ionic conductivity and polarity increase the absorption rate of microwave, which decrease the reaction time obviously. At the same time, in the microwave heater, the rapid-changing electrical field caused the ion polarization, which leads a temporary anisotropic micro-zone that develop the anisotropic growth of materials.

In summary, whilst originally developed as an effective green solvent for organic synthesis, these unique properties are being actively exploited in inorganic synthesis. For the thesis, because ionic liquids could react as template to control the morphology of materials and provide a non-aqueous reaction environment, 1-butyl-3-methylimidazolium acetate [BMIM](OAc) (shown as figure 8a) and 1-butyl-3-methylimidazolium dihydrogen phosphate [BMIM]H_2PO_4 (shown as figure 8b) ionic liquids were used for the synthesis of Ag_3PO_4 to control the morphology and improve the photoactivity.

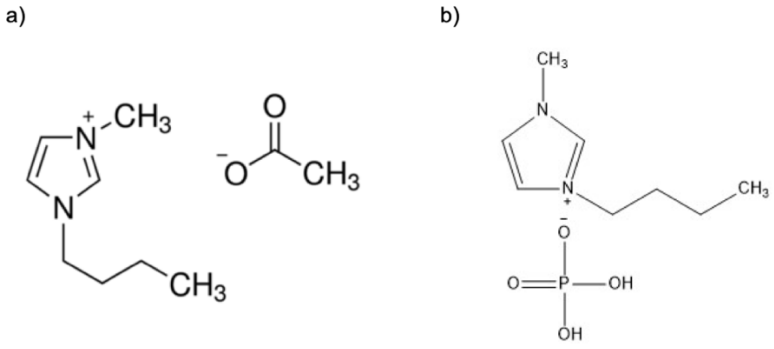

Figure 8. The molecular structures of a) 1-butyl-3-methylimidazolium acetate [BMIM](OAc) and b) 1-butyl-3-methylimidazolium dihydrogen phosphate [BMIM]H_2PO_4

Experimental

4. Materials preparation

Reactant	Molecular mass / g mol^{-1}	Source
Silver phosphate	169.87	99% purity, Sigma-Aldrich
Sodium dibasic phosphate	141.96	99% purity, Sigma-Aldrich
Ethanol	46.07	95% purity, Sigma-Aldrich
1-Butyl-3-methylimidazolium acetate [BMIM](OAc)	186.25	95% purity, Sigma-Aldrich
1-Butyl-3-methylimidazolium dihydrogen phosphate [BMIM]H2PO4	220.21	95% purity, Shanghai Chengjie
CM-Dextran sodium	1000-20000 (average M_w)	99% purity, Sigma-Aldrich

4.1. Synthesis of Silver phosphate in presence of CM Dextran

In a typical synthesis (Figure 9) , 1.8mmol of $AgNO_3$ was added to a 2ml 0.5wt.% solution of CM Dextran sodium salt in deionized water under rapid stirring and darkness for 2 hours. After addition of $AgNO_3$, the transparent CM Dextran sodium solution turned to a white dispersion immediately. After 2 hours stirring the white dispersion turned to a light yellow color. Then, 2ml 0.3mmol ml^{-1} of Na_2HPO_4 aqueous solution was added dropwise to the above dispersion, and bright yellow Ag_3PO_4 suspension should be formed. The suspension was stirred for a further 2 hours in darkness and became green color. Finally, the products were isolated by washing with deionized water and ethanol for 3 times and centrifuging, then the product was dried in convection oven at 80 ^oC for 24 hours to remove all moisture. To investigate the influence of CM Dextran in the Ag_3PO_4 synthesis, the above experiment was repeated with 1wt.%, 2wt.%, 5wt.% and 10wt.% CM Dextran

sodium aqueous solution. As control sample, an Ag_3PO_4 was synthesized with same concentration and condition as above, but in absence of CM Dextran sodium.

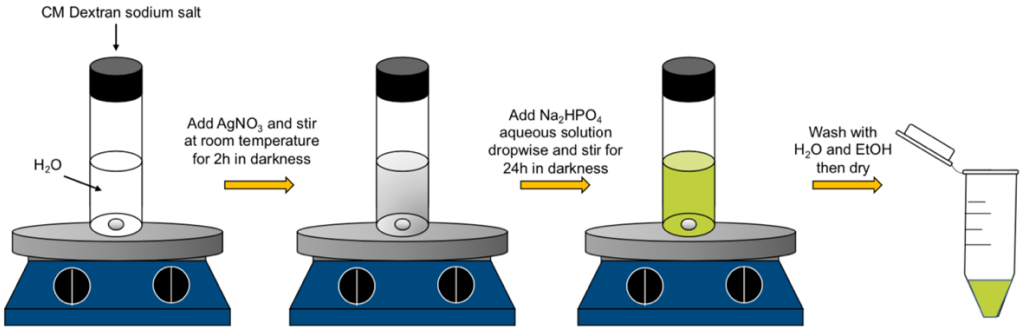

Figure 9. Schematic diagram of Ag_3PO_4 synthesis with CM Dextran sodium salt.

4.2. Synthesis of Silver phosphate using ionic liquid as a solvent

In a representative synthesis (Figure 10), 6mmol of $AgNO_3$ was added to 10ml 1-Butyl-3-methylimidazolium acetate [BMIM](OAc) and stirred rapidly in darkness for 24 hours. The $AgNO_3$ crystals were completely dissolved in the ionic liquid to produce a transparent $AgNO_3$-[BMIM](OAc) ionic liquid mixture. Subsequently, in a 7ml glass vial, 0.2mmol of 1-Butyl-3-methylimidazolium dihydrogen phosphate [BMIM]H_2PO_4 and 100µl of [BMIM](OAc) were mixed under rapid stirring and heated in high-temperature silicon oil bath at 120°C. After [BMIM]H_2PO_4 powder was completely melted, 1ml of the $AgNO_3$-[BMIM](OAc) ionic liquid mixture was pipetted to the [BMIM]H_2PO_4-[BMIM](OAc) ionic liquid mixture, and the final mixture kept stirring at 120°C in darkness for 2 hours. At the first 10 minutes, the transparent yellow mixture turned to dark brown suspension, however after 2 hours reaction, the mixture turned back to transparent bright yellow liquid. After removing from oil bath, the bright yellow liquid was cooled to room temperature and added with 500µl deionized water. With addition of water, yellow Ag_3PO_4 precipitate was yielded, and the yellow suspension was stirred in darkness for 24 hours. Finally, the product was washed and centrifuged with deionized water and ethanol for 3 times and dried in convection oven at 80°C for 24 hours. To investigate how reaction temperature and reactant concentration influence the formation of Ag_3PO_4, the above experiment was repeated with the conditions varied as presented in the Table 1.

Table 1. The conditions of contrast experiments for understanding the influence of reactant concentration and temperature on synthesis of Ag_3PO_4 with ionic liquids.

Label	Con. of $AgNO_3$-[BMIM](OAc)	Mole of $[BMIM]H_2PO_4$	Vol. of [BMIM](OAc) mixed with $[BMIM]H_2PO_4$	Reaction temperature
A_1	0.6mmol ml^{-1}	0.2mmol	100μl	120°C
A_2	0.6mmol ml^{-1}	0.2mmol	100μl	140°C
A_3	0.6mmol ml^{-1}	0.2mmol	100μl	160°C
B_1	0.9mmol ml^{-1}	0.3mmol	150μl	120°C
B_2	0.9mmol ml^{-1}	0.3mmol	150μl	140°C
B_3	0.9mmol ml^{-1}	0.3mmol	150μl	160°C
C_1	1.2mmol ml^{-1}	0.4mmol	200μl	120°C
C_2	1.2mmol ml^{-1}	0.4mmol	200μl	140°C
C_3	1.2mmol ml^{-1}	0.4mmol	200μl	160°C

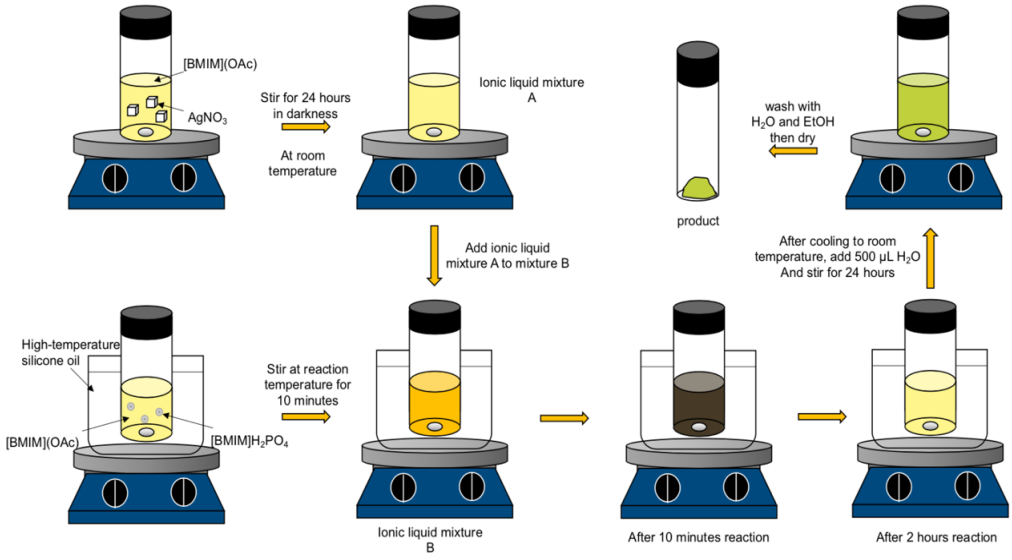

Figure 10. Schematic diagram of Ag_3PO_4 synthesis with ionic liquids.

5. Material characterization

Powder X-ray diffraction was characterized with D8 Advanced X-ray diffractometer (Bruker) using a Cu source with K_a = 1.5406Å. UV-Vis absorption spectra were measured with Perkin Elmer UV/Vis Lambda 750 spectrophotometer. The particle size and distribution are scaled by Zetasizer (Malvem Nano series) dynamic light

scattering. The Brunauer-Emmett-Teller test for specific surface area measurements was performed with Quantachrome Autosorb-iQ. Morphological characterization was performed using JEOL IT300 scanning electron microscope.

6. Experimental set-up for photooxidation of water

Water photooxidation reactions (Figure 1) were conducted in a special 75ml glass cell, and oxygen evolution was measured with a Neo Fox oxygen probe and processed with Ocean view software. The light source (150W MAX-303 Xenon lamp) with visible mirror model and full wavelength optical filter. To keep the illumination intensity the same in each experiment, the distance between the bottom of the glass cell and the head of the Xenon lamp was maintained at 20cm. 20mg Ag_3PO_4 and 85mg $AgNO_3$ were added to 50ml water with rapid stirring under darkness for 1 hour. The resultant bright yellow suspension was degassed with nitrogen in the glass cell until the value of oxygen concentration decreased to 0μmol L^{-1}. Following this, the light source was turned on and the value of oxygen evolution was recorded every 5 min over the period of 60 min. However, because the Neo Fox oxygen probe the oxygen concentration through fluorescence, the probe needle is sensitive to the light, which impact the data collection. Therefore, after every 5 min visible light irradiation, the light source was turned off for allowing the value to be stable and collected.

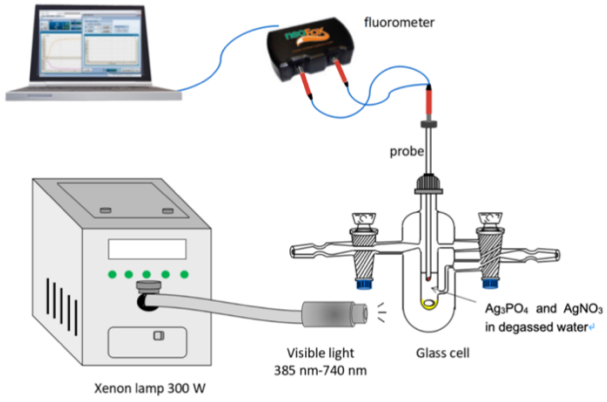

Figure 11. Schematic representation of experimental set-up of photooxidation measurement.

Result and discussion

7. CM Dextran mediated synthesis of Silver Phosphate

The long-chain structure and various functional groups, polymers are used for controlling synthesis of organic or inorganic materials. As shown in figure 12a, Zaheer [66] used amylose to control particle size and morphology of silver nanoparticles synthesis. After mixing $AgNO_3$ aqueous solution with ascorbic acid-starch mixture, silver ions could be absorbed on the outer surface of amylose, which is contributed by the long polymer chain structure of amylose and electrostatic interaction between positive charge of silver ions with lone pair electrons of -OH groups. beside this, Song [67] reported Ag cations absorption by the carbon nanospheres which surface was enriched with -OH and $-COO^-$ groups to increase chelation with silver ions (As shown in figure 12b). In the thesis, CM Dextran sodium salt was chosen for silver phosphate synthesis to control particle size and morphology. This is because that CM Dextran sodium salt possesses the long chain glucose polymer structure with abundant -OH and $-COO^-$ functional groups.

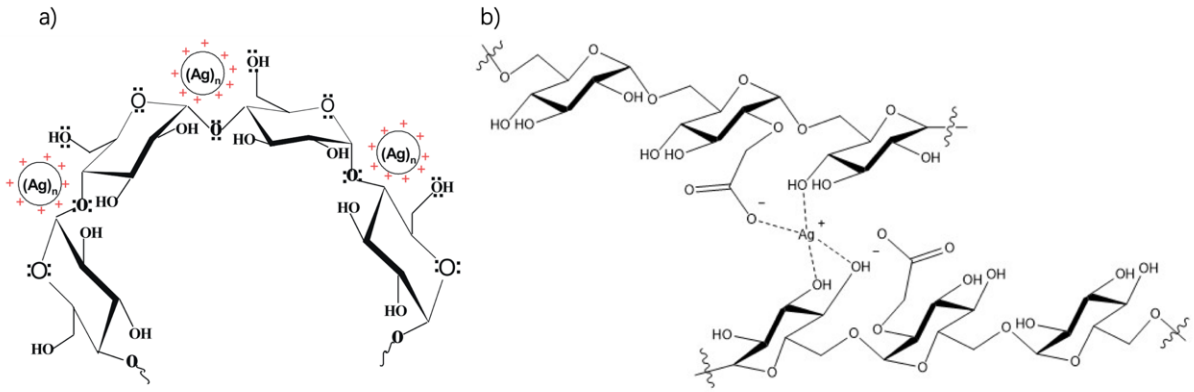

Figure 12. a) Absorption of silver ions on the outer surface of amylose. B) Chelation between -OH and $-COO^-$ groups with silver ions.

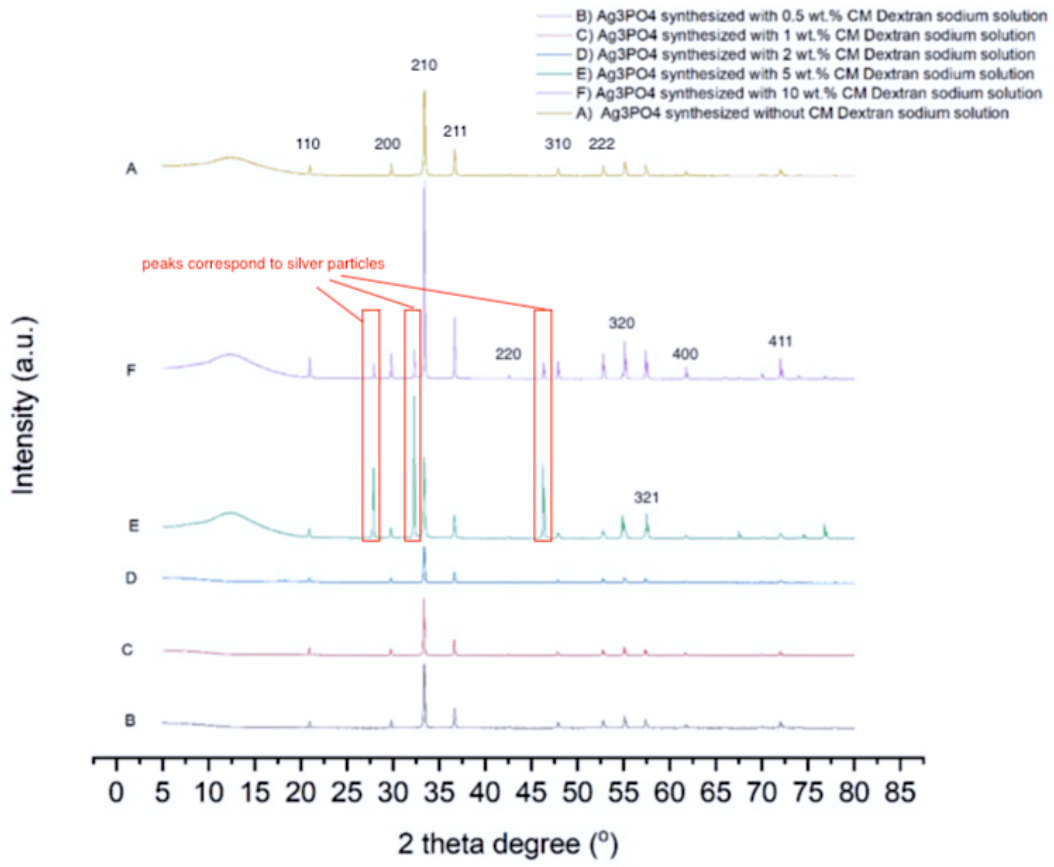

Figure 13. X-Ray diffraction patterns of silver phosphate synthesized A) without CM Dextran sodium; B) with 0.5wt.% C) 1wt.% D) 2wt.% E) 5wt.% F) 10wt.% of CM Dextran sodium aqueous solution.

In these experiments, aqueous dispersions of CM Dextran at different weight percentage were used to control the synthesis of silver phosphate. The products were firstly confirmed by PXRD. The XRD patterns in figure 13 were compared with JCPDS standard card, and they are completely corresponding to No. 06-0505 which is the body-centered cubic silver phosphate. The morphology of silver phosphate particles was observed by SEM. As shown in figure 14, the morphology of silver phosphate was altered with increase of CM Dextran sodium concentration. The Ag_3PO_4 (A) synthesized without CM Dextran sodium present irregular shape with a wide range of particle size, which is from approximately 15nm to 900nm. Then, after using 0.5wt.% CM Dextran sodium aqueous solution to control synthesis of Ag_3PO_4, the shape of product (B) turned to be spherical, but the particle size is still non-uniform. When weight percentage of CM Dextran sodium increase to 1wt.%, the shape and particle size tend to be uniform, the average

diameter of the Ag_3PO_4 (C) particle is approximately 307nm. Then, with 2wt.% CM Dextran sodium aqueous solution, the particle size of Ag_3PO_4 (D) reduced to about 260nm (diameter). However, further increase of CM Dextran sodium cannot control morphology and lower particle size of silver phosphate. Figure 14E and 14F showed SEM micrographs of Ag_3PO_4 synthesized with 5wt.% and 10wt.% CM Dextran sodium aqueous solution. Following with the increase of CM Dextran sodium, the particle size of Ag_3PO_4 became larger and non-uniform again, and the shape of crystal tended to be cubic.

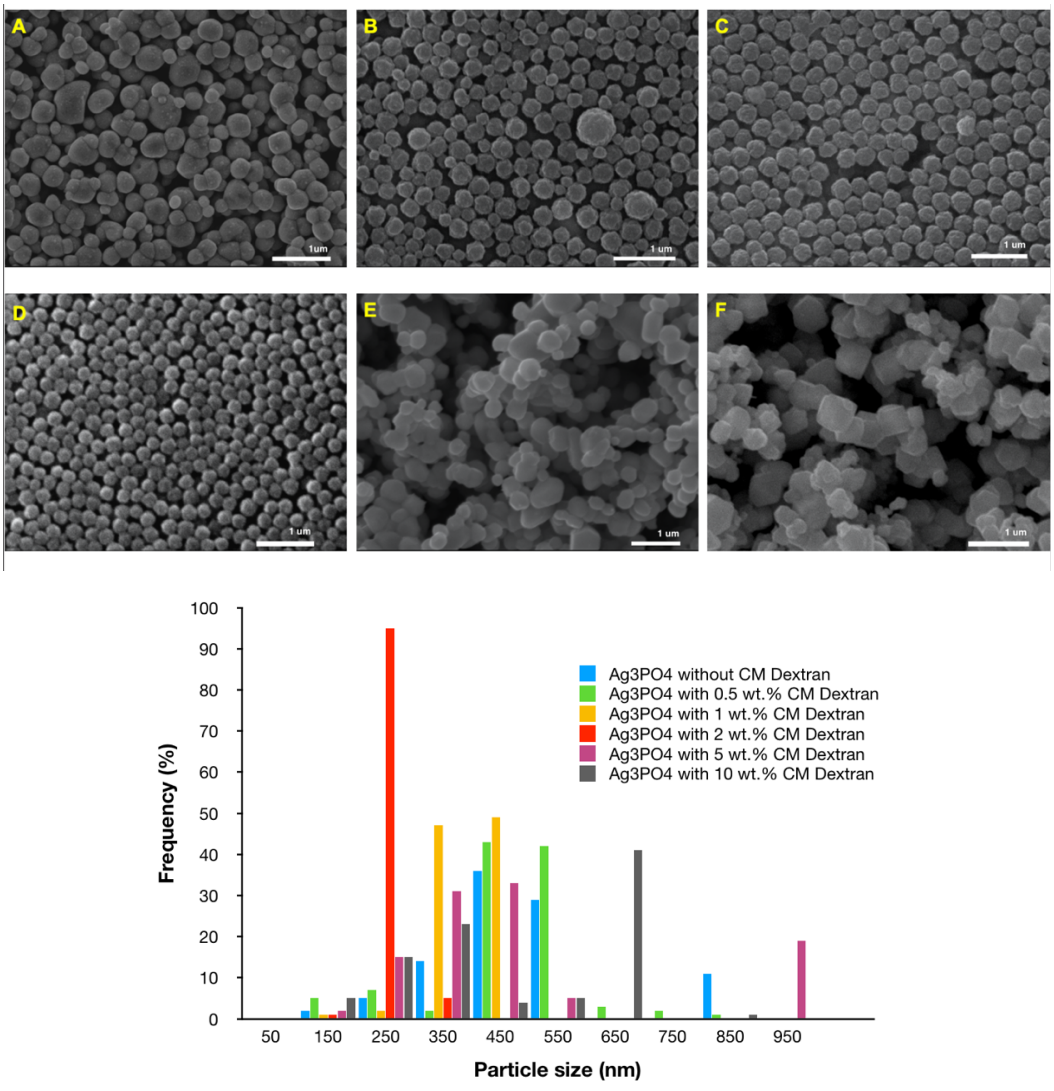

Figure 14. Top: SEM micrographs of silver phosphate synthesized A) without CM Dextran sodium; B) with 0.5wt.% C) 1wt.% D) 2wt.% E) 5wt.% F) 10wt.% of CM Dextran sodium aqueous solution. Bottom: The size distribution histogram of silver phosphate synthesized with different weight percentage CM Dextran aqueous solution.

The interaction between silver cation and CM Dextran sodium should play an important role in the morphology and particle size control of Ag_3PO_4. After $AgNO_3$ was mixed with CM Dextran sodium solution, a white semi-transparent dispersion was formed, which is caused by chelation between silver ions with $-COO^-$ group and electrostatic interaction between silver ions with oxygen element on CM Dextran. The CM Dextran reacted as both controlling agent and soft template in the reaction. Therefore, with a low concentration of CM Dextran facilitates the formation of monodisperse, Ag_3PO_4 particles with average size 260nm. However, when the concentration of the biopolymer increased, the reducibility of CM Dextran sodium impacted the silver cation in the solution [68]. Some silver ions could be reduced back to metallic silver particles, which affect the further reaction with phosphate anions and the morphology control. In the XRD patterns (Figure 13) of product C and D, beside the standard diffraction peaks of Ag_3PO_4, there are also some extra peaks showed around 27°, 32°, 46°, 55° and 57° for 2 theta degree, which are corresponding to the XRD pattern of silver particles. Furthermore, following with the shrink and enlarge of particle size, the surface area was also changed. Through BET measurement, the surface area of Ag_3PO_4 synthesized with 2wt.% CM Dextran is $9.4 m^2 g^{-1}$. Whereas, the surface area of Ag_3PO_4 synthesized without CM Dextran is only $2.2 m^2 g^{-1}$. The considerable increase of surface area could offer more active sites for the redox reactions on the surface of Ag_3PO_4.

Figure 15 shows the oxygen evolution of silver phosphate synthesized with different weight percentage CM Dextran sodium aqueous solution. After 60 minutes visible light irradiation, oxygen evolution of Ag_3PO_4 synthesized with 2wt.% CM Dextran sodium solution reached to 9870μmol g^{-1}, which is about 1.5 times of oxygen evolved by Ag_3PO_4 synthesized without CM Dextran sodium. Then, the oxygen evolution of silver phosphate synthesized with 0.5 and 1wt.% of CM Dextran sodium solution also presented significant development. However, there is no obvious improvement of oxygen evolution for Ag_3PO_4 synthesized with 5 and 10wt.% of CM Dextran sodium

solution.

Based on the experimental data analysis above, the improvement of photocatalytic activity should be contributed by the reduction of particle size and more uniform shape of Ag_3PO_4. The smaller particle size means a shorter distance for electrons and holes transition to surface. Therefore, the possibility of recombination could be reduced. And larger surface area provides more active sites for water photooxidation reaction. In conclusion, CM Dextran sodium could control morphology and particle size of Ag_3PO_4 to improve the photocatalytic activity through the chelation and electrostatic interaction between silver ions and CM Dextran sodium. But, due to the reducibility, CM Dextran sodium could reduce some silver ions, which impacts the morphology control and improvement of photocatalytic activity of Ag_3PO_4.

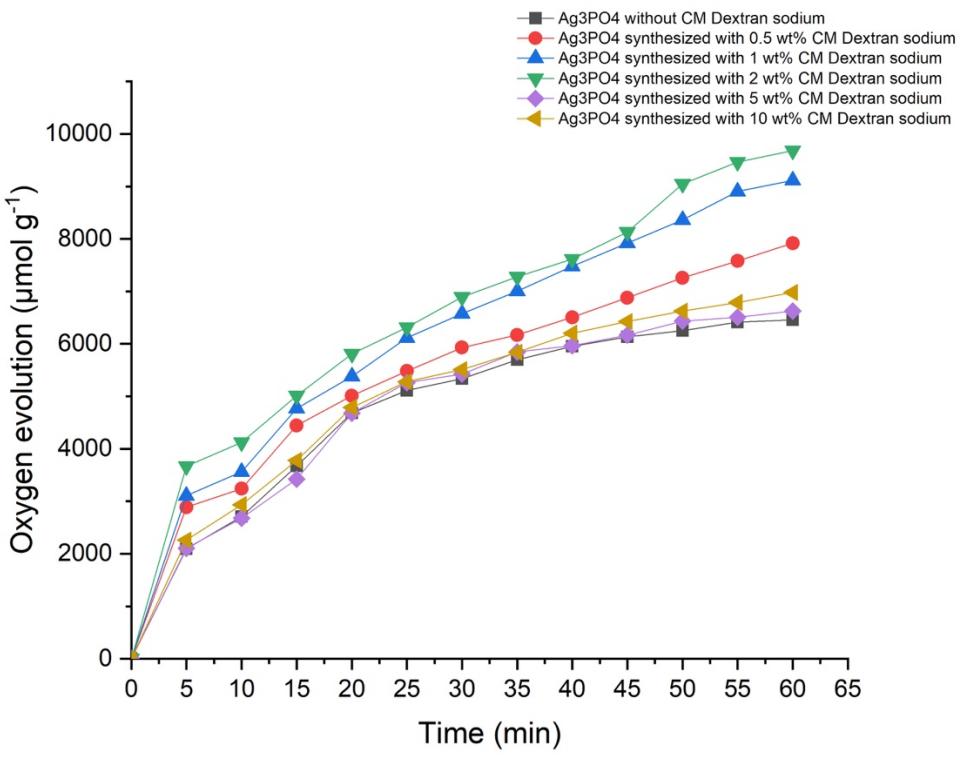

Figure 15. Oxygen yield comparison of Ag_3PO_4 synthesized with different weight percentage of CM Dextran sodium aqueous solution, which was tested by Neo Fox oxygen probe using 300W Xenon light source and $AgNO_3$ as sacrificial agent. (For each sample three reactions were performed, and average values are plotted)

8. Ionic liquid mediated synthesis of Silver Phosphate

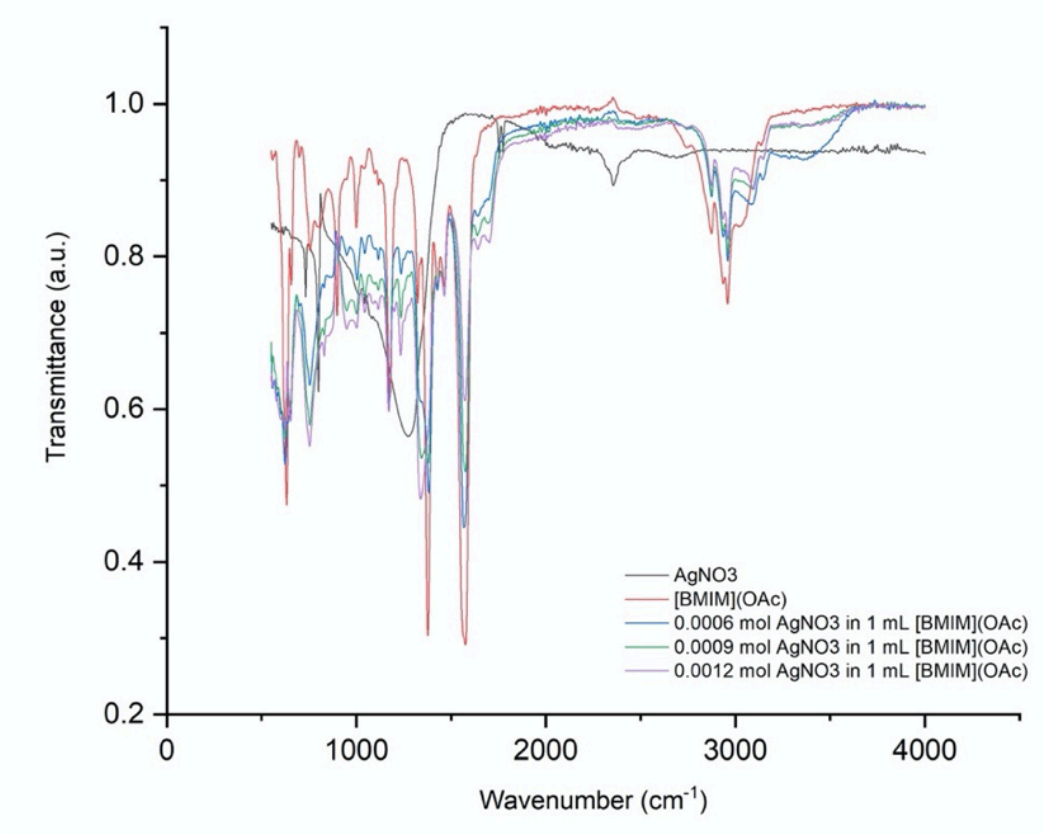

Figure 16. The FTIR spectra of $AgNO_3$, [BMIM](OAc) and $AgNO_3$-[BMIM](OAc) mixture with different mole of $AgNO_3$ (0.0006mole, 0.0009mole and 0.0012mole of $AgNO_3$).

In the experimental, $AgNO_3$ was dissolved in [BMIM](OAc) ionic liquids with long-time stir. And a suitable ionic liquid must be inert to the initial compound [69]. Therefore, the FTIR spectra were measured to confirm relationship between $AgNO_3$ and [BMIM](OAc) ionic liquid. As shown in figure 16, compared with FTIR spectra of $AgNO_3$ and [BMIM](OAc), there is no obvious new IR peak or peak shift of $AgNO_3$-[BMIM](OAc) mixture, which means [BMIM](OAc) is inert to $AgNO_3$. Then, because of the high melting point of [BMIM]H_2PO_4 (about 170^oC), a small volume of [BMIM](OAc) was added to lower the melting point of the [BMIM]H_2PO_4-[BMIM](OAC) ionic liquids mixture, which reduce the melting point to approximately 120^oC. The $AgNO_3$-[BMIM](OAc) and [BMIM]H_2PO_4-[BMIM](OAc) mixture were mixed and reacted in high-temperature oil bath for 2 hours at different temperature. The final mixture yielded dark brown precipitate firstly, then the precipitate turned

to dark green color, finally all precipitate totally re-dissolved into the liquid mixture and formed a yellow transparent liquid. After cooling down to room temperature, deionized water was introduced to the liquid mixture and yielded a yellow precipitate. PXRD patterns of the above samples are shown in Figure 17. The diffraction patterns showed a series of characteristic peaks associated with silver phosphate and were in good agreement with JCPDS standard (06-0505) corresponding to body-centered cubic silver phosphate. The cell parameter (a) is 6.026 Å [70], which confirms that all the products are silver phosphate without trace of other reactants or intermediate.

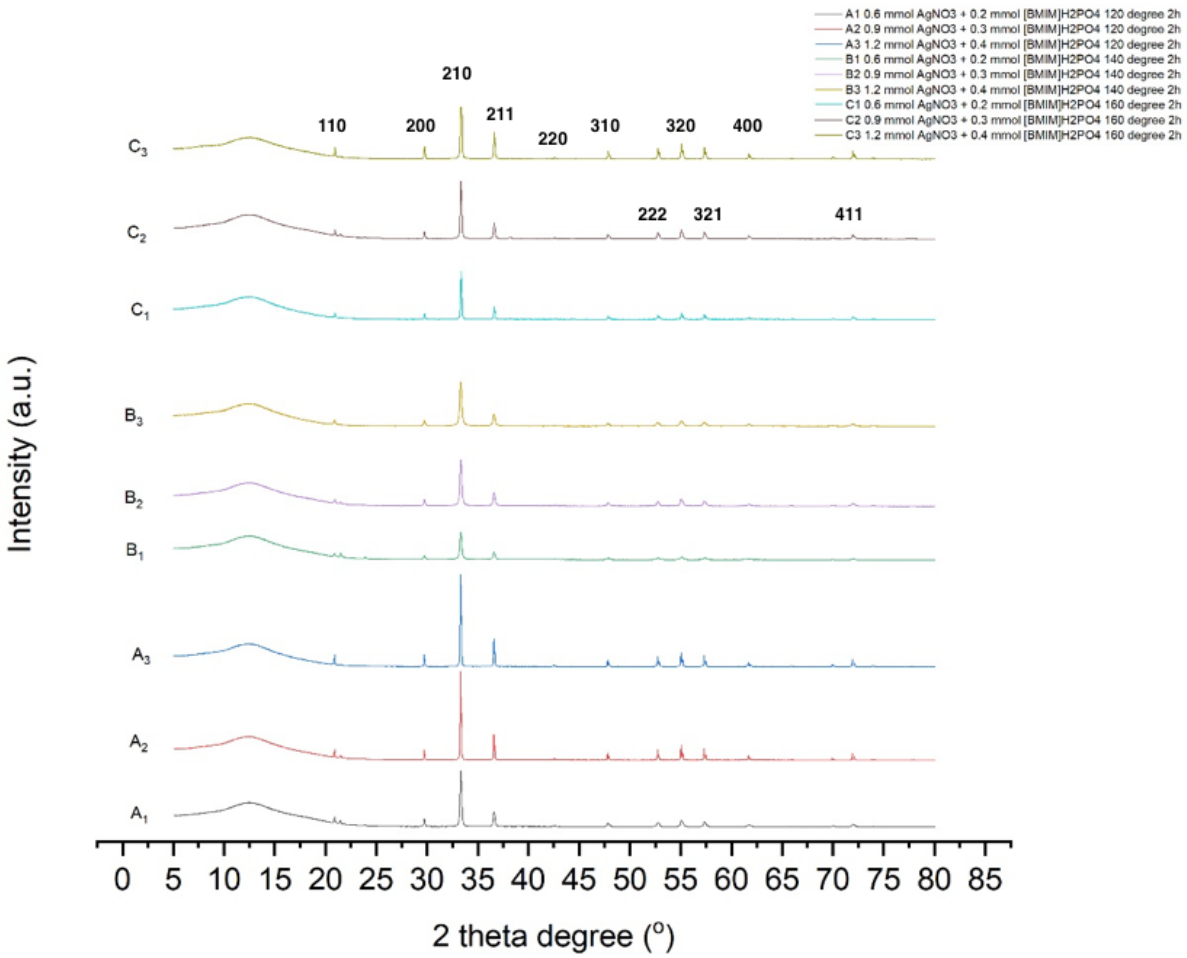

Figure 17. The XRD patterns of silver phosphate synthesized with different reaction condition. The labels A_1-C_3 are corresponding to labels of the products mentioned in Table 1 above.

The morphology of the silver phosphate crystals synthesized at different reaction temperatures was confirmed by SEM microscopy (Figure 19). The micrographs

show the influence of temperature and reactant concentration on the morphology of silver phosphate. Figure 18 shows the morphology of silver phosphate synthesized at room temperature in deionized water with 0.0006mol $AgNO_3$ and 0.0002mol $[BMIM]H_2PO_4$. The morphology of the Ag_3PO_4 is not regular and uniform. However, in figure 19, at different reaction temperature, Ag_3PO_4 shows various shapes. At 120°C, the morphology of the Ag_3PO_4 (A_1, A_2, A_3) tends to be rhombic dodecahedrons at all reactant concentrations. However, when reaction temperature is raised to 160°C, the morphology of the Ag_3PO_4 (C_1, C_2, C_3) tends to be trisoctahedron following with reactants concentration increasing. In contrast, if the reaction is kept at 140°C for 2 hours, the morphology of Ag_3PO_4 (B_1, B_2, B_3) presents as flower-like shape. To investigate whether any of the observed morphology changes might demonstrate enhanced photocatalysis BET surface area measurements were conducted. As shown in table 2, the flower-like Ag_3PO_4 structure possess considerably larger surface area (34.5m^2 g^{-1}), which is about 17 times larger than control sample (Ag_3PO_4 synthesized in water at room temperature). The surface area is also significantly enhanced compared to the more geometric crystals produced at 120 and 160 degree. Before adding water to the final reacted liquid mixtures, all liquid mixtures look similar, which are all bright yellow transparent sticky liquids. However, after addition of water, the Ag_3PO_4 was produced and showed distinct morphologies and properties. In these experiments, 500µl deionized water was added dropwise to the liquid mixture with rapid stirring, no immediate color change was observed the Ag_3PO_4 did not yield at the beginning, but after adding all 500µl deionized water the entire transparent liquid mixture suddenly turned to yellow suspension. There are two possible assumptions of the synthesis principle. 1) There are already exist Ag_3PO_4 nanoparticles dispersing in the liquid mixture, after adding water, the nanosized Ag_3PO_4 particles reacted as precursor and form micro-sized Ag_3PO_4 crystals with different morphology. 2) Before addition of water, there are silver cations and phosphate anions in the liquid mixture. After addition of water to the reaction mixture, the behavior of ionic liquids changes from a solvent to co-solute, thereby pronouncing the accumulation

tendency of the individual ions at the interface [71]. Therefore, silver ions and phosphate ions accumulate together and yield silver phosphate precipitate in water phase.

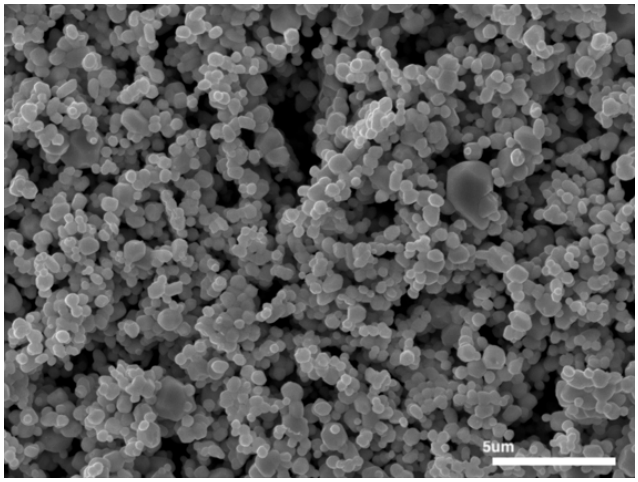

Figure 18. The SEM micrograph of Ag_3PO_4 synthesized with 1ml of 0.0006mol ml^{-1} of $AgNO_3$ aqueous solution and 1ml of 0.0002mol ml^{-1} of NaH_2PO_4 aqueous solution react at 25°C for 2 hours.

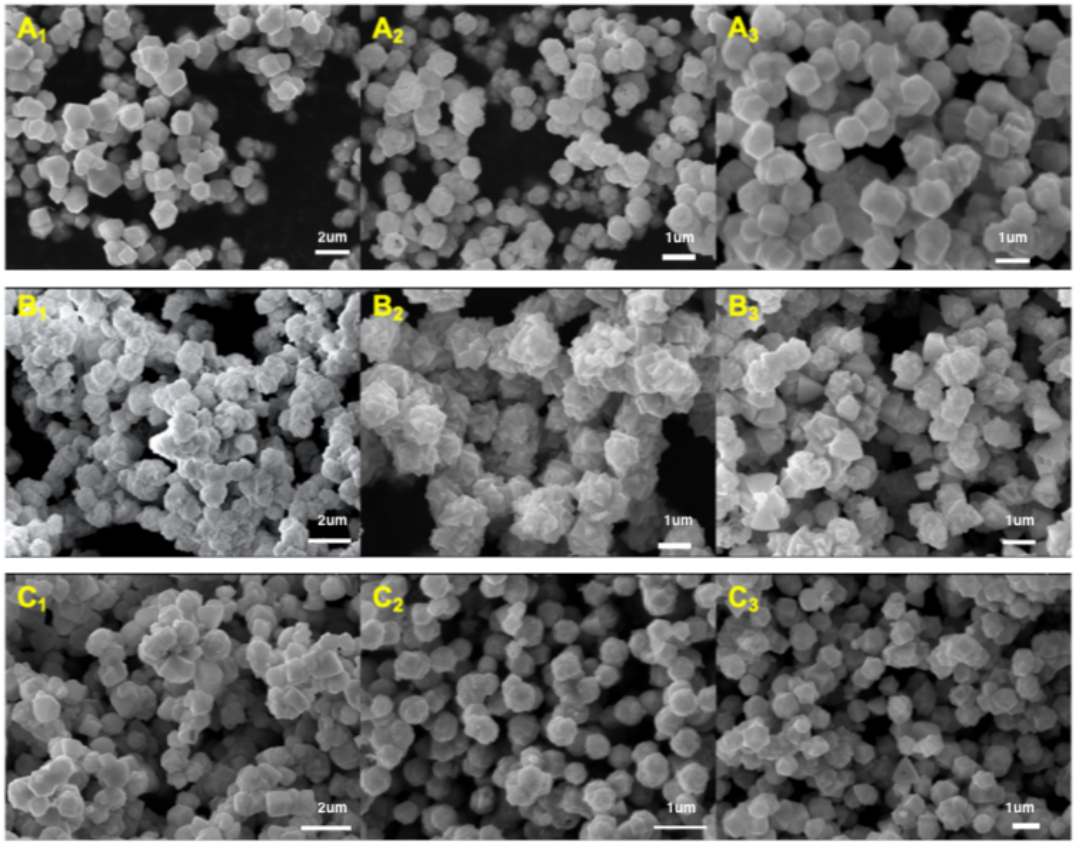

Figure 19. The SEM micrographs of Ag_3PO_4 synthesized with different reaction condition. The labels A_1-C_3 are corresponding to labels of the products mentioned in Table 1 above.

Table 2. Specific surface area measured by BET of different Ag_3PO_4.

Ag_3PO_4	Specific surface area / $m^2\ g^{-1}$
Synthesized in water	2.1
A_1	2.3
A_2	2.8
A_3	2.5
B_1	31.9
B_2	36.5
B_3	27.7
C_1	3.1
C_2	3.4
C_3	3.7

As discussed in the introduction section, because of the position of valance band and conduction band of Ag_3PO_4, the photocatalyst find applications in photo-oxidation of water. In this study, the Ag_3PO_4 produced is used as a photocatalyst that could catalyse oxidation of water in presence of the sacrificial agent (AgNO3) under visible light illumination. The oxygen evolution was measured with Neo Fox oxygen probe. Compared with gas chromatograph measurement, the Neo Fox oxygen probe is easier to use and monitor the oxygen concentration during the photocatalytic reaction. However, in the past research about water photooxidation, Neo Fox oxygen probe is not a popular measurement instrument. Therefore, to make the data more reliable and comparable, a standard control sample of Ag_3PO_4 was synthesized using reported recipe [9] and was tested with Neo Fox oxygen probe. The oxygen evolution of the mixed-faceted Ag_3PO_4 is 4520μmol g^{-1}. But the oxygen evolution reported by Martin [9] is about 1600μmol g^{-1}, which was measured with gas chromatograph. Then with some other contrast experiments, it seems that the value of oxygen evolution tested with Neo Fox probe is approximately 3 times larger than the value measured with gas chromatograph.

The photocatalytic activities of Ag_3PO_4 samples prepared at various temperature conditions are presented in figure 20. Compared to the control sample (Ag_3PO_4 synthesized in water at room temperature, the oxygen evolution is 6060μmol g^{-1}),

all Ag_3PO_4 synthesized with ionic liquids perform better in water photooxidation. Significantly, per gram of Ag_3PO_4 synthesized in ionic liquids at 140^oC for 2 hours showed 15230μmol oxygen in an hour, which is 251% more than the control sample. After considering the difference between probe methods (gas chromatograph and NeoFox oxygen probe), the Ag_3PO_4 synthesized in ionic liquids at 140^oC for 2 hours yield about double volume of oxygen evolving by the modified tetrahedrons Ag_3PO_4 reported by Martin and co-workers. The development of the photocatalytic activity should be caused by the increase of surface area and morphology control. To investigate the recyclability of the catalyst and test the photocatalytic stability of the Ag_3PO_4 in the water photooxidation reaction, each Ag_3PO_4 sample was reused in the photocatalytic reaction. After each cycle of photooxidation reaction, extra $AgNO_3$ was added to the reaction system to supplement sacrificial agent the new suspension was degassed again. As shown in figure 21, the total oxygen evolution recorded every 60 minutes of Ag_3PO_4 synthesized in water decreased in line with the increase of reaction rounds. Interestingly, the oxygen evolution rate of Ag_3PO_4 synthesized in ionic liquids was not impacted by the increase of reaction rounds. The reduction of photocatalytic activity could be caused by the formation of silver particles during water photooxidation. For the reactions occurring on the surface of Ag_3PO_4 crystals, the photo-induced holes react with H_2O molecules and yield oxygen gas, simultaneously, the photo-induced electrons react with Ag^+ ions providing by $AgNO_3$ and yield silver particles which could aggregate at the surface of Ag_3PO_4 and hinder the light absorption [72]. Furthermore, the oxygen evolution of silver phosphate increased in the second or even third cycle of the water photooxidation reaction. The reason could be that the trace amount of metallic silver particles formed on the Ag_3PO_4 surface previously modified the Ag-Ag_3PO_4 system. Because silver possesses a lower Fermi level than Ag_3PO_4, a Schottky junction would form at the interface between silver and silver phosphate. The photoelectrons could migrate from Ag_3PO_4 to the metallic silver which could act as a temporary electron reservoir. [73] As a result, the recombination between photo-

induced electrons and holes could be restrained and the photocatalytic activity will improve.

Beside the photocatalytic stability, the scale of silver phosphate may also influence the oxygen evolution measurement. Because the unit of oxygen evolution in the figures is μmol per gram, but in the experiment, only 20mg of Ag_3PO_4 was used for water photooxidation test. It cannot be confirmed that the oxygen evolution will increase linearly with larger amount of Ag_3PO_4. However, due to the high cost of ionic liquids, it is too expensive to synthesize grams of Ag_3PO4 for this investigation. Therefore, as shown in figure 22, the 20, 50, 100 and 200mg of an Ag_3PO_4 synthesized in ionic liquids were taken water photooxidation measurement respectively. Within same reaction time, the relationship between oxygen evolution and quantity of silver phosphate is linear. Thus, there are reasons to believe that the oxygen evolution values shown in figure 20 and 21 are relatively accurate.

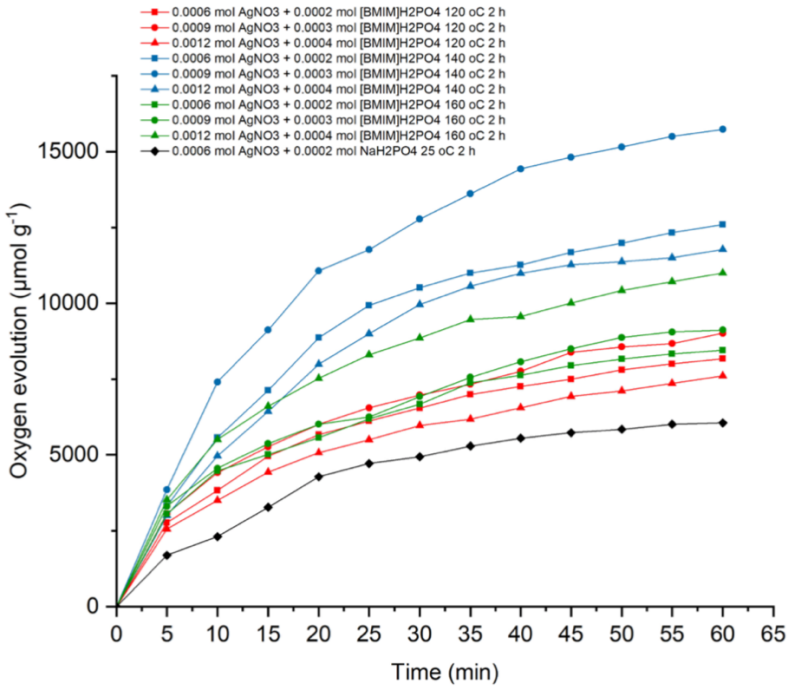

Figure 20. The oxygen yield comparison of Ag_3PO_4 synthesized in ionic liquids with different reactant concentration and temperature, which was tested by Neo Fox oxygen probe using 300W Xenon light source and $AgNO_3$ as sacrificial agent.(For each sample three reactions were pperformed,and average values are plotted)

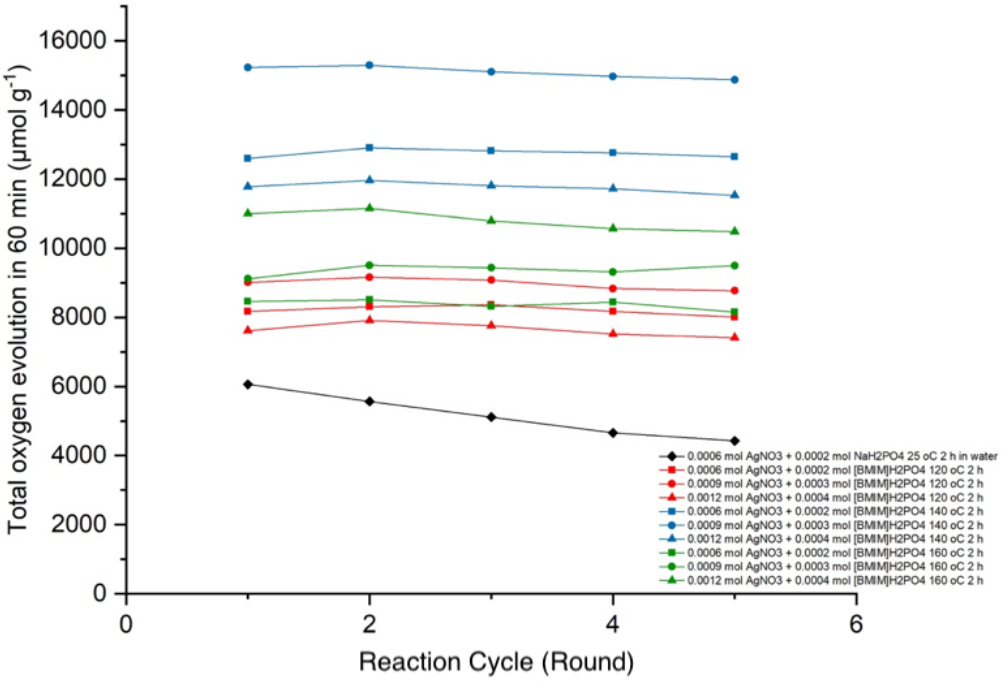

Figure 21. Photocatalytic stability test with four more rounds of water photooxidation reactions. After each reaction, 50mg $AgNO_3$ was added for the next round of the reaction.

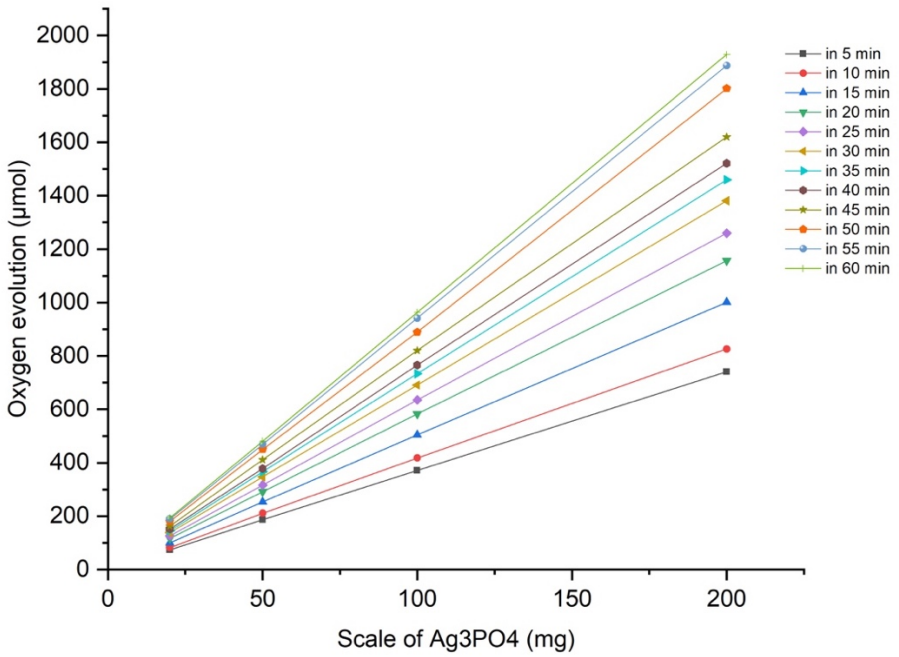

Figure 22. The oxygen yield comparison of 20mg, 50mg, 100mg and 200mg Ag_3PO_4 synthesized with 0.6mmol ml^{-1} of $AgNO_3$-[BMIM](OAc) and 0.2mmol of [BMIM]H_2PO_4 at 140°C for 2 hours within same reaction time.

According to analysis above, ionic liquids could control the morphology of silver phosphate with different reaction temperature, and the considerable increase of specific surface area provides more active sites for oxidation reaction with H_2O. Considering the two previous hypotheses of Ag_3PO_4 formation from ionic liquid mixture, it seems that the Ag_3PO_4 with variable morphology should be guided with different precursors. Because, in the comparison experiments, the differences between the morphology and size of Ag_3PO_4 synthesized at the same temperature but different reactants concentration is not obvious. However, with the same concentration of reactants, different reaction temperature makes the final Ag_3PO_4 product present extremely different shape and surface area. Further the ratio between the ionic liquid mixture and additional water is kept constant in each experiment. Therefore, the entropy change caused by water addition should be similar in different experiments, which cannot alter the formation of silver phosphate and control morphology. In conclusion, after 2 hours of high temperature reaction, different nanosized Ag_3PO_4 particles formed in ionic liquids and acted as precursors to further Ag_3PO_4 crystallization. Furthermore, the difference between the Ag_3PO_4 precursors should be caused by the change of physical property of ionic liquids. Following with the increase of temperature, the density, refractive index, surface tension, dynamic and kinetic viscosities will change [74]. Therefore, the putative nanosized Ag_3PO_4 precursors are also different. Then, the additional water made ions and particles aggregate on the interface between water and ionic liquids, which led to the final Ag_3PO_4 crystals formation. Unlike other inorganic material synthesis with ionic liquids, the high melting of [BMIM]H_2PO_4 means the reaction cannot occur at room temperature. However, it also provides an opportunity to understand the synthesis of inorganic material with ionic liquids at high temperature (over 100^{o}C).

Conclusion and future works

In this study two novel methods were developed to enhance the photoactivity of silver phosphate. Firstly, CM Dextran sodium solution and ionic liquids were used to control the particle size and morphology of Ag_3PO_4. The chelation and electrostatic interaction between silver ions with hydroxyl and carboxylic groups could decrease the particle size of the Ag_3PO_4 and the shape of particles tend to be uniformly spherical. With 2wt.% CM Dextran sodium aqueous solution, the diameter of Ag_3PO_4 particles is lowered to about 260nm and present as uniform spheres. However, if the weight percentage of CM Dextran sodium solution was further increased, because the reducibility of CM Dextran sodium to the silver ions, the metallic silver particles impact the formation of Ag_3PO_4.

Then, the ionic liquids were used as both solvent and reactant in the synthesis of Ag_3PO_4. The [BMIM](OAc) was used to dissolve $AgNO_3$ and mixed with [BMIM]H_2PO_4 to lower the melting point of [BMIM](OAc)- [BMIM]H_2PO_4 mixture. After reacting at 120^{o}C, 140^{o}C and 160^{o}C for 2 hours, the reaction mixture was transparent. Then, with 500μL water addition, yellow Ag_3PO_4 precipitate was formed, and the different reaction temperature led Ag_3PO_4 with totally distinct morphology. During the reaction, there should be several different Ag_3PO_4 nanoparticles formed and dispersing in the ionic liquid mixture. After introducing water to the reaction system, silver cations and phosphate anions were aggregated and the Ag_3PO_4 nanoparticles worked as precursor for the further crystal production. For the reactions happened at 120^{o}C and 160^{o}C, the Ag_3PO_4 crystal tended to be rhombic dodecahedrons and trisoctahedron respectively, and compared with multifaced Ag_3PO_4 crystal, they present higher activity in water photooxidation. More specially, for the reactions happened at 140^{o}C, the morphology of Ag_3PO_4 is a flower-like shape. The unique morphology provided Ag_3PO_4 crystal with significantly larger surface area, which also increased the oxygen evolution under visible light irradiation. The oxygen evolution of the silver phosphate synthesized with CM Dextran and ionic liquids achieved 2 to 3 times increase, compared with

control samples. Significantly, the photocatalyst is recyclable and retained its photocatalytic activity even after four reaction cycles. With several repeated reaction cycles test, the stability of the silver phosphate was also proved to be increased by the morphology control.

For the future work, the influence of other polymers to the morphology control of silver phosphate could be studied. Furthermore, the feasibility of applying the synthesis methods to other types of photocatalyst is also worth to be investigated. Then, according to literature reference, synthesis of the hollow Ag_3PO_4 nanospheres in ionic liquids with assistance of surfactant could be possible. The hollow spherical structure could increase surface area and shorten the distance for electrons and holes transition to surface, which could improve photoactivity. Furthermore, photooxidation is just a half reaction of water splitting. Therefore, combining Ag_3PO_4 with another semiconductor for photoreduction to form a complete photoelectrical cell is an important target.

Reference

1. Ellabban, O., Abu-Rub, H. and Blaabjerg, F. (2014). Renewable energy resources: Current status, future prospects and their enabling technology. Renewable and Sustainable Energy Reviews, 39, pp.748-764.
2. Kudo, A. and Miseki, Y. (2009). Heterogeneous photocatalyst materials for water splitting. Chem. Soc. Rev., 38(1), pp.253-278.
3. Eibner, Alexander (1911). "Action of Light on Pigments I". Chem-ZTG. 35: 753–755.
4. FUJISHIMA, A. and HONDA, K. (1972). Electrochemical Photolysis of Water at a Semiconductor Electrode. Nature, 238(5358), pp.37-38.
5. Amano F (2020). Visible Light Responsive Pristine Metal Oxide Photocatalyst: Enhancement of Activity by Crystallization Under Hydrothermal Treatment. NCBI, pp.17650-17651.
6. Devi, L. and Kavitha, R. (2013). A review on non-metal ion doped titania for the photocatalytic degradation of organic pollutants under UV/solar light: Role of photogenerated charge carrier dynamics in enhancing the activity. Applied Catalysis B: Environmental, 140-141, pp.559-587.
7. Zhang, K. and Guo, L. (2013). Metal sulphide semiconductors for photocatalytic hydrogen production. Catalysis Science & Technology, 3(7), p.1672.
8. Kang, Y., Yang, Y., Yin, L., Kang, X., Liu, G. and Cheng, H. (2015). An Amorphous Carbon Nitride Photocatalyst with Greatly Extended Visible-Light-Responsive Range for Photocatalytic Hydrogen Generation. Advanced Materials, 27(31), pp.4572-4577.
9. Martin, D., Liu, G., Moniz, S., Bi, Y., Beale, A., Ye, J. and Tang, J. (2015). Efficient visible driven photocatalyst, silver phosphate: performance, understanding and perspective. Chemical Society Reviews, 44(21), pp.7808-7828.
10. Khan, Z., Chetia, T., Vardhaman, A., Barpuzary, D., Sastri, C. and Qureshi, M. (2012). Visible light assisted photocatalytic hydrogen generation and organic dye degradation by CdS–metal oxide hybrids in presence of graphene oxide. RSC Advances, 2(32), p.12122.

11. Saravanan, R., Gracia, F. and Stephen, A. (2017). Basic Principles, Mechanism, and Challenges of Photocatalysis. Nanocomposites for Visible Light-induced Photocatalysis, pp.19-40.
12. Suchea, M., Tudose, I., Koudoumas, E., Tiganescu, V. and Codita, I. (2019). TiO2-based nanostructured materials with germicidal properties and other applications in biomedical fields. Functional Nanostructured Interfaces for Environmental and Biomedical Applications, pp.323-339.
13. Sunlight, UV and accelerated weathering. (1988). Additives for Polymers, 18(7), p.3.
14. Pan, J. and Liu, G. (2017). Facet Control of Photocatalysts for Water Splitting. Semiconductors and Semimetals, pp.349-391.
15. Habisreutinger, S.N. Schmidt-Mende, L. Stolarczyk, J.K. Photocatalytic reduction of CO2 on TiO2 and other semiconductors, Angew. Chem. Int. Ed. 52 (29) (2013) 7372–7408.
16. Tran, P.D. Recent advances in hybrid photocatalysts for solar fuel production, Energy Environ. Sci. 5 (3) (2012) 5902–5918.
17. Wang, K. et al., Sulfur-doped g-C3N4 with enhanced photocatalytic CO2- reduction performance, Appl. Catal. B 176–177 (2015) 44–52.
18. Wang, B. Yang, H.T. Xian, Di, L. J.R.S. Li, X.X. Wang, Synthesis of spherical Bi2WO6 nanoparticles by a hydrothermal route and their photocatalytic properties, J. Nanomater. (2015) 1–7.
19. Low, J., Yu, J., Jaroniec, M., Wageh, S. and Al-Ghamdi, A. (2017). Heterojunction Photocatalysts. *Advanced Materials*, 29(20), p.1601694.
20. Tian, N., Huang, H., Liu, C., Dong, F., Zhang, T., Du, X., Yu, S. and Zhang, Y. (2015). In situ co-pyrolysis fabrication of CeO2/g-C3N4 n–n type heterojunction for synchronously promoting photo-induced oxidation and reduction properties. *Journal of Materials Chemistry A*, 3(33), pp.17120-17129.
21. Zhou, W., Sun, F., Pan, K., Tian, G., Jiang, B., Ren, Z., Tian, C. and Fu, H. (2011). Well-Ordered Large-Pore Mesoporous Anatase TiO2 with Remarkably High Thermal Stability and Improved Crystallinity: Preparation, Characterization, and

Photocatalytic Performance. *Advanced Functional Materials*, 21(10), pp.1922-1930.

22. Martin, D., Umezawa, N., Chen, X., Ye, J. and Tang, J. (2013). Facet engineered Ag3PO4 for efficient water photooxidation. *Energy & Environmental Science*, 6(11), p.3380.
23. Yi, Z., Ye, J., Kikugawa, N., Kako, T., Ouyang, S., Stuart-Williams, H., Yang, H., Cao, J., Luo, W., Li, Z., Liu, Y. and Withers, R. (2010). An orthophosphate semiconductor with photooxidation properties under visible-light irradiation. *Nature Materials*, 9(7), pp.559-564.
24. Martin, D., Liu, G., Moniz, S., Bi, Y., Beale, A., Ye, J. and Tang, J. (2015). Efficient visible driven photocatalyst, silver phosphate: performance, understanding and perspective. *Chemical Society Reviews*, 44(21), pp.7808-7828.
25. Bi, Y., Hu, H., Ouyang, S., Lu, G., Cao, J. and Ye, J. (2012). Photocatalytic and photoelectric properties of cubic Ag3PO4 sub-microcrystals with sharp corners and edges. *Chemical Communications*, 48(31), p.3748.
26. Preston, C., Xu, Y., Han, X., Munday, J. and Hu, L. (2013). Optical haze of transparent and conductive silver nanowire films. *Nano Research*, 6(7), pp.461-468.
27. Wang, J., Teng, F., Chen, M., Xu, J., Song, Y. and Zhou, X. (2013). Facile synthesis of novel Ag3PO4tetrapods and the {110} facets-dominated photocatalytic activity. *CrystEngComm*, 15(1), pp.39-42.
28. Chen, X., Huang, X. and Yi, Z. (2014). Enhanced Ethylene Photodegradation Performance of g-C3N4-Ag3PO4Composites with Direct Z-Scheme Configuration. *Chemistry - A European Journal*, 20(52), pp.17590-17596.
29. Xie, J., Yang, Y., He, H., Cheng, D., Mao, M., Jiang, Q., Song, L. and Xiong, J. (2015). Facile synthesis of hierarchical Ag 3 PO 4 /TiO 2 nanofiber heterostructures with highly enhanced visible light photocatalytic properties. *Applied Surface Science*, 355, pp.921-929.

30. Cao, J., Luo, B., Lin, H., Xu, B. and Chen, S. (2012). Visible light photocatalytic activity enhancement and mechanism of AgBr/Ag3PO4 hybrids for degradation of methyl orange. *Journal of Hazardous Materials*, 217-218, pp.107-115.
31. Saison, T., Chemin, N., Chanéac, C., Durupthy, O., Ruaux, V., Mariey, L., Maugé, F., Beaunier, P. and Jolivet, J. (2011). Bi2O3, BiVO4, and Bi2WO6: Impact of Surface Properties on Photocatalytic Activity under Visible Light.
32. Kang, Z., Zhang, X., Chen, Y., Akram, M., Nie, J. and Zhu, X. (2017). Preparation of polymer/calcium phosphate porous composite as bone tissue scaffolds. *Materials Science and Engineering: C*, 70, pp.1125-1131.
33. Yang, G., Hou, W., Feng, X., Xu, L., Liu, Y., Wang, G. and Ding, W. (2007). Nanocomposites of Polyaniline and a Layered Inorganic Acid Host: Polymerization of Aniline in the Layers, Conformation, and Electrochemical Studies. *Advanced Functional Materials*, 17(3), pp.401-412.
34. Sun, J., Jordan, L., Forsyth, M. and MacFarlane, D. (2001). Acid–Organic base swollen polymer membranes. *Electrochimica Acta*, 46(10-11), pp.1703-1708.
35. Yang, C., Hsu, S. and Chien, W. (2005). All solid-state electric double-layer capacitors based on alkaline polyvinyl alcohol polymer electrolytes. *Journal of Power Sources*, 152, pp.303-310.
36. Schlapschy, M., Theobald, I., Mack, H., Schottelius, M., Wester, H. and Skerra, A. (2007). Fusion of a recombinant antibody fragment with a homo-amino-acid polymer: effects on biophysical properties and prolonged plasma half-life. *Protein Engineering Design and Selection*, 20(6), pp.273-284.
37. Buchko, C., Chen, L., Shen, Y. and Martin, D. (1999). Processing and microstructural characterization of porous biocompatible protein polymer thin films. *Polymer*, 40(26), pp.7397-7407.
38. Taylor, L. and Zografi, G. (1998). Sugar–polymer hydrogen bond interactions in lyophilized amorphous mixtures. *Journal of Pharmaceutical Sciences*, 87(12), pp.1615-1621.
39. Jang, J. and Bae, J. (2005). Fabrication of mesoporous polymer using soft template method. *Chemical Communications*, (9), p.1200.

40. CALCIUM OXALATE FILMS ON STONE SURFACES: EXPERIMENTAL ASSESSMENT OF THE CHEMICAL FORMATION. (2019).
41. Pu, S., Zinchenko, A. and Murata, S. (2011). Conformational behavior of DNA-templated CdS inorganic nanowire.
42. Mecerreyes, D. (2011). Polymeric ionic liquids: Broadening the properties and applications of polyelectrolytes. *Progress in Polymer Science*, 36(12), pp.1629-1648.
43. Doyle, M., Choi, S. and Proulx, G. (2000). High-Temperature Proton Conducting Membranes Based on Perfluorinated Ionomer Membrane-Ionic Liquid Composites. *Journal of The Electrochemical Society*, 147(1), p.34.
44. Berthod, A., Ruiz-Ángel, M. and Carda-Broch, S. (2008). Ionic liquids in separation techniques. *Journal of Chromatography A*, 1184(1-2), pp.6-18.
45. Mehnert, C. (2005). Supported Ionic Liquid Catalysis. *Chemistry - A European Journal*, 11(1), pp.50-56.
46. Kurig, H., Vestli, M., Tõnurist, K., Jänes, A. and Lust, E. (2012). Influence of Room Temperature Ionic Liquid Anion Chemical Composition and Electrical Charge Delocalization on the Supercapacitor Properties. *Journal of The Electrochemical Society*, 159(7), pp.A944-A951.
47. Freire, M., Carvalho, P., Fernandes, A., Marrucho, I., Queimada, A. and Coutinho, J. (2007). Surface tensions of imidazolium based ionic liquids: Anion, cation, temperature and water effect. *Journal of Colloid and Interface Science*, 314(2), pp.621-630.
48. Gutel, T., Garcia-Antõn, J., Pelzer, K., Philippot, K., Santini, C., Chauvin, Y., Chaudret, B. and Basset, J. (2007). Influence of the self-organization of ionic liquids on the size of ruthenium nanoparticles: effect of the temperature and stirring. *Journal of Materials Chemistry*, 17(31), p.3290.
49. Zhang, S., Sun, N., He, X., Lu, X. and Zhang, X. (2006). Physical Properties of Ionic Liquids: Database and Evaluation. *Journal of Physical and Chemical Reference Data*, 35(4), pp.1475-1517.

50. Brandt, A., Ray, M., To, T., Leak, D., Murphy, R. and Welton, T. (2011). Ionic liquid pretreatment of lignocellulosic biomass with ionic liquid–water mixtures. *Green Chemistry*, 13(9), p.2489.
51. Ballesteros-Gómez, A., Sicilia, M. and Rubio, S. (2010). Supramolecular solvents in the extraction of organic compounds. A review. *Analytica Chimica Acta*, 677(2), pp.108-130.
52. Ao, M., Huang, P., Xu, G., Yang, X. and Wang, Y. (2008). Aggregation and thermodynamic properties of ionic liquid-type gemini imidazolium surfactants with different spacer length. *Colloid and Polymer Science*, 287(4), pp.395-402.
53. Ma, Z., Yu, J. and Dai, S. (2010). Preparation of Inorganic Materials Using Ionic Liquids. *Advanced Materials*, 22(2), pp.261-285.
54. Wang, C., Li, A., Xu, J., Wen, J., Zhang, H. and Zhang, L. (2019). Preparation of WO 3 /CNT catalysts in presence of ionic liquid [C 16 mim]Cl and catalytic efficiency in oxidative desulfurization. *Journal of Chemical Technology & Biotechnology*, 94(10), pp.3403-3412.
55. Parnham, E., Drylie, E., Wheatley, P., Slawin, A. and Morris, R. (2006). Ionothermal Materials Synthesis Using Unstable Deep-Eutectic Solvents as Template-Delivery Agents. *Angewandte Chemie International Edition*, 45(30), pp.4962-4966.
56. ZHANG, G., TAO, L. and ZHANG, G. (2008). Effect of Hydrophobic Carbon Chain Length on the Crystal Structure of MCM-41. *Chinese Journal of Chemical Engineering*, 16(4), pp.631-634.
57. Fonseca, G., Machado, G., Teixeira, S., Fecher, G., Morais, J., Alves, M. and Dupont, J. (2006). Synthesis and characterization of catalytic iridium nanoparticles in imidazolium ionic liquids. *Journal of Colloid and Interface Science*, 301(1), pp.193-204.
58. Jutz, F., Andanson, J. and Baiker, A. (2009). A green pathway for hydrogenations on ionic liquid-stabilized nanoparticles. *Journal of Catalysis*, 268(2), pp.356-366.
59. Huang, J., Jiang, T., Gao, H., Han, B., Liu, Z., Wu, W., Chang, Y. and Zhao, G. (2004). Pd Nanoparticles Immobilized on Molecular Sieves by Ionic Liquids:

Heterogeneous Catalysts for Solvent-Free Hydrogenation. *Angewandte Chemie International Edition*, 43(11), pp.1397-1399.

60. Kim, k., Demberelnyamba, D. and Lee, H. (2004). Size-selective synthesis of gold and platinum nanoparticles using novel thiol-functionalized ionic liquids.
61. Itoh, H., Naka, K. and Chujo, Y. (2004). Synthesis of Gold Nanoparticles Modified with Ionic Liquid Based on the Imidazolium Cation. *Journal of the American Chemical Society*, 126(10), pp.3026-3027.
62. Lazarus, L., Riche, C., Malmstadt, N. and Brutchey, R. (2012). Effect of ionic liquid impurities on the synthesis of silver nanoparticles.
63. Zhao, X., Jin, W., Cai, J., Ye, J., Li, Z., Ma, Y., Xie, J. and Qi, L. (2011). Shape- and Size-Controlled Synthesis of Uniform Anatase TiO2 Nanocuboids Enclosed by Active {100} and {001} Facets. *Advanced Functional Materials*, 21(18), pp.3554-3563.
64. Choi, H., Kim, Y., Varma, R. and Dionysiou, D. (2006). Thermally Stable Nanocrystalline TiO2 Photocatalysts Synthesized via Sol−Gel Methods Modified with Ionic Liquid and Surfactant Molecules.
65. Nakashima, T. and Kimizuka, N. (2003). Interfacial Synthesis of Hollow TiO2 Microspheres in Ionic Liquids.
66. Zaheer, Z., Aazam, E. and Hussain, S. (2016). Reversible encapsulation of silver nanoparticles into the helix of amylose (water soluble starch). *RSC Advances*, 6(65), pp.60513-60521.
67. Song, X., Gunawan, P., Jiang, R., Leong, S., Wang, K. and Xu, R. (2011). Surface activated carbon nanospheres for fast adsorption of silver ions from aqueous solutions. *Journal of Hazardous Materials*, 194, pp.162-168.
68. Lim, E., Jang, E., Kim, J., Lee, T., Kim, E., Park, H., Suh, J., Huh, Y. and Haam, S. (2012). Self-fabricated dextran-coated gold nanoparticles using pyrenyl dextran as a reducible stabilizer and their application as CT imaging agents for atherosclerosis. *Journal of Materials Chemistry*, 22(34), p.17518.
69. Gao, R., Song, J., Hu, Y., Zhang, X., Gong, S. and Li, W. (2017). Facile Synthesis of Ag/Ag3 PO4 Composites with Highly Efficient and Stable Photocatalytic

Performance under Visible Light. *Journal of the Chinese Chemical Society*, 64(10), pp.1172-1180.

70. Liu, J., Luo, C., Wang, J., Yang, X. and Zhong, X. (2012). Controlled synthesis of silver phosphate crystals with high photocatalytic activity and bacteriostatic activity. *CrystEngComm*, 14(24), p.8714.
71. Ratti, R. (2014). Ionic Liquids: Synthesis and Applications in Catalysis. *Advances in Chemistry*, 2014, pp.1-16.
72. Zaheer, Z., Aazam, E. and Hussain, S. (2016). Reversible encapsulation of silver nanoparticles into the helix of amylose (water soluble starch). *RSC Advances*, 6(65), pp.60513-60521.
73. Wan, J., Liu, E., Fan, J., Hu, X., Sun, L., Tang, C., Yin, Y., Li, H. and Hu, Y. (2015). In-situ synthesis of plasmonic Ag/Ag3PO4 tetrahedron with exposed {111} facets for high visible-light photocatalytic activity and stability. *Ceramics International*, 41(5), pp.6933-6940.
74. Lim, E., Jang, E., Kim, J., Lee, T., Kim, E., Park, H., Suh, J., Huh, Y. and Haam, S. (2012). Self-fabricated dextran-coated gold nanoparticles using pyrenyl dextran as a reducible stabilizer and their application as CT imaging agents for atherosclerosis. *Journal of Materials Chemistry*, 22(34), p.17518.